Replacement Insulation Gas for SF6

Matthew Brown

Durban, December 22, 2016

In fulfilment of the Masters of Science, College of Agriculture, Engineering and Science, University of KwaZulu-Natal.

As the candidates Supervisor I agree to the submission of this dissertation.

Signed on 14/12/2017

_____

Dr A.G. Swanson

Declaration 1 - Plagiarism

I, Matthew Daniel Brown declare that

1. The research reported in this dissertation is, except where otherwise indicated, my original research.
2. This dissertation has not been submitted for any degree or examination at any other university.
3. This dissertation does not contain other persons' data, pictures, graphs or other information, unless specifically acknowledged as being sourced from other persons.
4. This dissertation does not contain other persons' writing, unless specifically acknowledged as being sourced from other researchers. Where other written sources have been quoted, then:
    a. Their words have been re-written but the general information attributed to them has been referenced.
    b. Where their exact words have been used, then their writing has been placed inside quotation marks, and referenced.
5. To the best of my knowledge this dissertation does not contain text, graphics or tables copied and pasted from the Internet, unless specifically acknowledged, and the source being detailed in the dissertation and in the References sections.

Signed on 22/12/2016

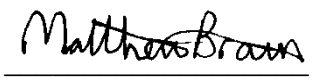

Matthew Daniel Brown

Declaration 2 - Publications

DETAILS OF CONTRIBUTION TO PUBLICATIONS that form part and/or include research presented in this dissertation:

Publication 1

M.D. Brown, A.G. Swanson and L. Jarvis. *Mean Energy, Electron Drift and Effective Ionisation Coefficients in SF_6 - N_2 Mixtures from Bolsig+*. SAUPEC, Vereeniging, 6A-2, 2016

Publication 2

C. Babunandan, M.D. Brown and A.G. Swanson. *Impulse Breakdown of SF_6 - N_2 Gas Mixtures*. SAUPEC, Vereeniging, 6A-3, 2016

Publication 3

M.D. Brown, A.G. Swanson and L. Jarvis. *Drift-Diffusion Modelling of Breakdown of SF_6 Mixtures*. ISH, Buenos Aires, 2017

The experimental work performed in **Publication 1** was performed by Matthew Brown with aid from Andrew Swanson. The report was authored by M.D. Brown and co-authored by Andrew Swanson and Leigh Jarvis.

The experimental work in **Publication 2** was performed by Matthew Brown with the aid of Chasheral Babunandan. The report was authored by Chasheral Babunandan and co-authored by Matthew Brown and Andrew Swanson.

The experimental work performed in **Publication 3** was performed by Matthew Brown with aid from Andrew Swanson. The report was authored by M.D. Brown and co-authored by Andrew Swanson and Leigh Jarvis.

Signed on 22/12/2016

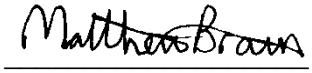

Matthew Daniel Brown

Abstract

This dissertation investigates the synergy of the SF_6-N_2/CO_2 mixtures under lightning impulse (LI) conditions on the basis of the fundamental processes and dynamic behaviour of gas discharge.

The gas processes associated with the breakdown behaviour and the synergy of the mixtures are investigated, where a Boltzmann equation solver, the electron energy distribution function (EEDF) and the Townsend and transport coefficients are used to understand the phenomena and provide input to a flux corrected transport model. A one and a half dimension Flux Corrected Transport – Finite Difference Method (1.5D FCT-FDM) model is used to account for the dynamic behaviour of the gas discharge. The solver and model clearly indicate synergy effects under steady state and dynamic conditions respectively. Experimental measurements were performed for comparison.

Under LI voltages and uniform field conditions the breakdown of the SF_6-N_2 and SF_6-CO_2 mixtures increase with pressure. Breakdown under negative LI tends to be higher than breakdown under positive impulse for both mixtures. The synergy effects are dependent on polarity of the LI and SF_6 content of the mixture. Stronger synergistic effects are observed under negative LI. SF_6-N_2 mixtures demonstrate stronger synergy effects at low SF_6 content (<25%) while SF_6-CO_2 mixtures have stronger synergy effects at higher SF_6 content (>50%). Contrary to both the Boltzmann solver and the model results, the experimental results showed that the SF_6-CO_2 mixtures tended to demonstrate higher breakdown voltage than the SF_6-N_2 mixtures.

Together the modelled and experimental results indicate that the synergy of a gas mixture is strongly dependant on the dynamic behaviour of gas discharge.

Acknowledgements

I would like to thank my family and friends for their support throughout my studies. I would also like to thank my supervisor Dr Andrew Swanson for his encouragement and advice and my co-supervisor Dr Leigh Jarvis for his input.

Table of Contents

Table of Figures

1 Introduction

Sulphur Hexafluoride (SF_6) is a strongly electronegative gas, has a high dielectric strength and due to the large amount of energy required to decompose and maintain an arc in it, it possesses excellent arc-quenching properties. In addition, SF_6 is non-toxic, chemically inert and non-flammable enabling safe handling and long lived gas insulated equipment.

As a result, since the 1960s SF_6 has been the dominant gaseous electrical insulating and arc-quenching medium used in the electric power industry [1] [2].

Unfortunately SF_6 is the most potent greenhouse gas known, with a Global Warming Potential (GWP) of almost 24 000, and due to a lifespan of 3 200 years the SF_6 leaked into the atmosphere (during manufacture, service, recovery and disposal) is cumulative and effectively permanent as illustrated in Figure 1 [1] [2] [3] [4] [5] [6].

This resulted in SF_6 being one of the six controlled gases included in the Kyoto protocol [7]. In addition to its environmental impact, SF_6 is expensive, sensitive to non-uniform electric fields, forms toxic compounds under electrical discharge and demonstrates non-ideal gas behaviour at low temperatures.

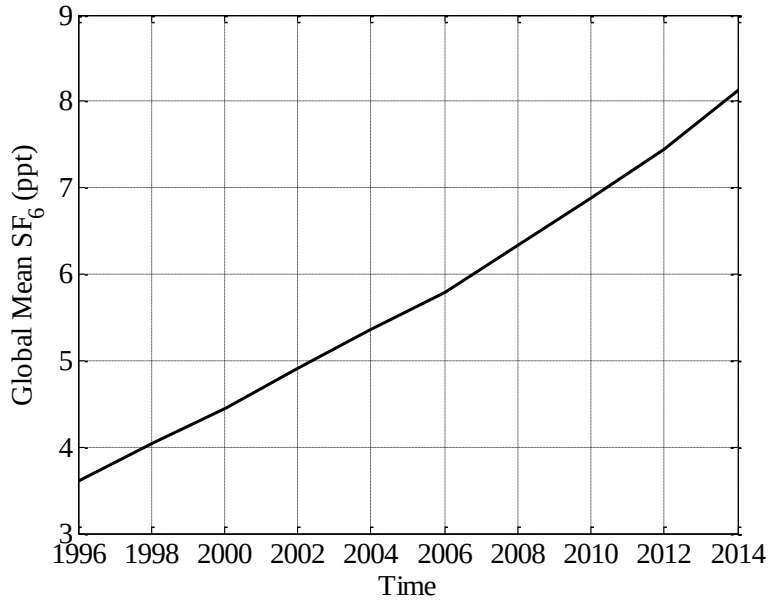

Figure 1: The development of the global mean atmospheric content of SF_6 [3]

This combination of environmental, economic and performance factors have fuelled a drive to find an alternative to SF_6. In the 1970s and 1980s the focus of research was to find an alternative possessing superior insulation properties, however, the focus of the current research is to find a comparable dielectric gas with significantly reduced environmental impact [8] [9] [10]. A detailed compilation of SF_6 alternatives is given by Christophorou, Olthoff and Green [8].

In general a replacement gas must meet the following criteria among others [3] [8]:

- Physical and chemical:
    - High dielectric strength
    - Good arc-quenching capabilities (high thermal conductivity and fast recovery)
    - Low boiling point and high vapour pressure at operating temperature
    - High heat dissipation
    - Chemically inert
- Health and safety:
    - Non-toxic
    - Non-flammable
    - No harmful decomposition products
    - Easy handling
- Environmental:
    - No ozone depletion potential
    - Low GWP

Many of the requirements a gaseous medium must meet such as high dielectric strength, chemical inertness and low toxicity tend to be mutually exclusive [8] [11] [12]. Gases with a high dielectric strength are strongly attaching (electronegative) gases but strongly attaching gases tend to be toxic, chemically reactive, environmentally unfriendly and possess high boiling points [3]. Environmentally friendly gases on the other hand, which are benign, abundant and cheap, have low attaching capabilities therefore low dielectric strengths.

The difficulty of finding a pure replacement gas that meets these requirements has resulted in a shift to instead find a gas mixture as a replacement for SF_6. The addition of the environmentally friendly or "buffer" gases to the strongly electronegative gases

lowers the boiling point of the mixture and reduces the environmental impact (GWP) [3]. Christophorou et al [8] [13] [14] believe that the most viable gas mixture to replace pure SF_6 is a SF_6 mixture with a "buffer" gas that enables the reduction of the GWP of the mixture while still maintaining dielectric properties comparable to that of pure SF_6.

In addition, investigations conducted over the past few decades found that some SF_6 mixtures exhibit a desirable positive synergy effect, whereby the component gases act together to improve the dielectric performance to greater than the sum of the components [10] [15] [16]. This synergistic effect is highly desirable in a gaseous mixture.

However, while the dielectric strength of mixtures exhibiting synergistic properties may tend towards that of pure SF_6, the arc-quenching properties of the mixtures tend to be significantly lower than that of pure SF_6 [1]. As a result the SF_6 and buffer gas mixtures are only viable replacements where dielectric strength and not arc-quenching is the primary concern, such as in gas insulated lines [2].

Both Nitrogen (N_2) and Carbon Dioxide (CO_2) are considered as viable additives to SF_6 as they are benign, abundant, cheap and exhibit a positive synergy effect when mixed with SF_6. SF_6-N_2 mixtures are already being used in gas insulated lines [3] and in cold climates where pure SF_6 deviates from ideal gas behaviour [9].

1.1 Aim of this Work

The aim of this research is the investigation of the efficiency of the synergy effect in SF_6-N_2/CO_2 gas mixtures under the application of lightning impulse (LI) voltages. The pure gases and their mixtures are examined from a physics point of view with the theory of electron behaviour considered the dominant role in a gaseous discharge. The Boltzmann equation is then used to analyse the interaction of the gases under steady state conditions and calculate the swarm parameters. A one and a half dimension Flux Corrected Transport – Finite Difference Method (1.5D FCT-FDM) model (developed by Swanson [17]) is used to account for the dynamic behaviour of the gas discharge. The modelled results are then experimentally validated under positive and negative LI voltages for varying SF_6 concentrations and pressures under uniform field conditions.

2 Theory of Gas Discharge and Breakdown

In its normal state a dielectric gas is a perfect insulator. However, upon the application of a sufficiently high electric field to a gas insulated system, free electrons can gain energy and cause ionisation [18]. If a sufficient fraction of electrons cause ionisation, gas discharge occurs [18] [19] [20] [21]. Should positive feedback occur between the primary and secondary effects of electrical discharge, the non-sustained discharge will transition to a self-sustained discharge and breakdown will occur.

The initiation and propagation of the gas discharge is controlled by the development of charged particles and their transport characteristics. The development and transport of the charged particles in the gas are dependent on the nature, number density and temperature of the gas, the nature of the applied voltage and the electrode geometry, separation, surface condition and material.

2.1 Fundamental Processes in Gas Discharge

There are a number of complex processes involving electrons, positive ions, negative ions, excited molecules, neutral molecules and photon interactions within the gas and with the electrodes which affect the dielectric behaviour of an insulating gas [22]. The dominant effect of these processes on the dielectric behaviour of an electrically stressed gas is due to their impact on the electron production, depletion and scattering processes [13] [14] [18] [19] [20] [23] [24].

2.1.1 Electron Production Processes

The probability of an electric discharge being initiated is dependent on the probability of a free electron appearing.

Free electrons may be formed in a number of ways [1]:

- Through the ionisation of neutral molecules by cosmic and terrestrial radiation. In gas insulated systems this is the main source of seed electrons [20].
- By electron detachment from negative ions. This is the main source of seed electrons in electronegative gases [20].
- As a result of electrode field emission.

In electronegative gases, all the free electrons can be captured by the gas molecules to form negative ions. This leads to the belief that in stressed electronegative gases the dominant source of breakdown-initiating free electrons is due to electron detachment from negative ions [20] [23]. Therefore, in a highly stressed gas the highest probability of breakdown occurs near the positive electrode [20].

2.1.1.1 Electron Ionisation

2.1.1.1.1 Electron Impact Ionisation

Electron impact ionisation occurs when a free electron collides with a neutral gas molecule resulting in the release of a new free electron and the production of a positive ion. In strong electric fields ionisation by electron impact is the most important process leading to breakdown [25]. Generally, there are two electron-impact ionisation processes [14] [20]:

- Direct impact ionisation:

$$e + XY \rightarrow XY^{+} + 2e$$

- Dissociative ionisation:

$$e + XY \rightarrow X(X)^{*} + Y^{+} + 2e$$

For ionisation by collision to occur the free electron must possess energy greater than or equal to the ionisation energy of the neutral molecule:

$$e^{-} + X \xrightarrow{\varepsilon \geq eV_i} 2e^{-} + X^{+} \tag{1}$$

Where:

$$\varepsilon = energy\ gained \text{ (eV)}$$

$$eV_i = ionisation\ energy \text{ (eV)}$$

This may lead to the assumption that if a gas has a low ionising energy (is easily ionised) the gas would possess a low dielectric strength. However; the breakdown strength of the dielectric gas does not directly correlate with the ionisation energy. Instead the breakdown strength is associated with the frequency at which ionisation collisions occur [25]. This ionisation frequency is related to the probability of an ionisation collision occurring on impact and the number of free electrons [26].

To cause ionisation ε must be at least equal to the ionisation energy of the molecule (eV_i). However, as ionisation is a stochastic process not all collisions with $\varepsilon \geq eV_i$ will cause ionisation.

2.1.1.1.2 Photo-ionisation

Photo-ionisation may occur either directly or indirectly.

$$hv + XY \rightarrow XY^{+} + e$$

Photo-ionisation occurs directly when the amount of radiant energy absorbed by the neutral molecule exceeds the ionisation energy of the molecule resulting in the photon causing the ejection of one or more electrons known as photoelectrons [21]. Photo-ionisation occurs directly when:

$$\lambda \leq c \cdot \frac{h}{V_i} \tag{2}$$

Where:

$h = Planck's\ constant$

$c = velocity\ of\ light$ ($\mathrm{m} \cdot \mathrm{s}^{-1}$)

$\lambda = incident\ radiation\ wavelength$ (m)

$V_i = ionisation\ energy$ (eV)

Photo-ionisation occurs indirectly when an electron does not possess sufficient energy to cause ionisation but excites the molecule without freeing an electron. When the excited molecule returns to its ground state it releases a photon. This photon in turn may ionise a particle in the process of photo-ionisation.

$$e + XY \rightarrow XY^{*} + e$$

$$XY^{*} \rightarrow XY + hv$$

The role of indirect photo-ionisation is likely to be insignificant in relation to the other processes [20].

2.1.1.1.3 Thermal ionisation

At sufficiently high temperatures gas molecules may be excited to such a high energy that upon collision with other molecules ionisation occurs. In flames and high pressure arcs this is the principle source of ionisation [1].

2.1.1.2 Electron Detachment

Once a free electron has become attached to a molecule it is no longer free to participate in further ionisation. In order for the attachment process to be most effective, the attached electron should not detach easily as electron detachment is the key mechanism responsible for the production of breakdown initiating electrons in electronegative gases [20] [23].

2.1.1.2.1 Auto Detachment:

$$X^{-*} \rightarrow X + e + energy$$

In this process, the negative ion is unstable due to excess internal energy. If the E/N value lies below the critical value $(E/N)_{lim}$ then this process is not significant [20].

2.1.1.2.2 Field-Induced Detachment:

$$X^{-} \rightarrow X + e$$

In this process, the electric field is strong enough to cause the electron to be removed from the negative ion; however, this process is unlikely for fields that are below 10 MV/cm [20].

2.1.1.2.3 Collisional Detachment:

$$X^{-} + Y \rightarrow X + Y + e$$

$$X^{-} + Y \rightarrow XY + e$$

Collisional detachment is the most likely mechanism for the detachment process should the ion gain a threshold kinetic energy approximately twice the EA of the negative ion [20].

2.1.1.2.4 Photo-detachment

In photo-detachment a photon collides with a negative ion to release an electron.

$$X^{-} + hv \rightarrow X + e$$

2.1.1.3 Electron Detachment by Positive and Metastable Ion Impact

Electrons may be emitted from metal surfaces under impact of positive and metastable ions. This occurs when the colliding ion releases two electrons from the surface: one to neutralise the ion and the other as the emitted electron. In order to do this the energy of the ion (the sum of the kinetic and potential energy) must be greater than twice the work function of the metal [20].

$$W_p + W_k \geq 2W_a \tag{3}$$

Where:

$$W_a = work\ function\ of\ the\ metal$$

$$W_p = potential\ energy\ of\ the\ ion$$

$$W_k = kinetic\ energy\ of\ the\ ion$$

2.1.1.4 Photoelectric emission

Upon impact with the cathode surface photons with a sufficiently high energy may eject an electron if the photon energy exceeds the work function of the metal. The work function for common elements is given in Table 1.

Table 1: Work function for common elements [1]

Element	W_a (eV)
Ag	4.74
Al	2.98 - 4.43
Cu	4.07 - 4.70
Fe	3.91 - 4.60
W	4.35 - 4.60

2.1.2 Electron Depletion Processes

2.1.2.1 Electron Attachment

In a strong insulator the free electrons are efficiently attached to prevent their participation in the breakdown process. The most common attachment processes are recombination and negative ion formation. During the recombination processes free electrons may be joined with positive ions while during negative ion formation electrons become attached to electronegative molecules. The ions have too great a mass to be sufficiently accelerated by the electric field thus do not result in ionisation collisions.

2.1.2.1.1 Recombination

Upon collision free electrons and positive ions will recombine and a photon will be released. The recombination rate is dependent on the concentration of the positive ions and electrons [1].

$$X^+ + e \rightarrow X + hv$$

2.1.2.1.2 Negative ion formation

The dominant negative ion formation is: direct attachment and dissociative attachment. In direct attachment an "electron directly attaches to form negative ion" while in dissociative attachment "the molecules split into their constituent atoms and the electronegative atom forms a negative ion" [27].

The electron attachment process is considered one of the most important micro processes in determining the breakdown strength of a gas [20] [22]. In general the strongly attaching (electronegative) gases have a higher breakdown strength than the weakly attaching and non-attaching gases [10] [21] . Electronegative gases are able to attach a free electron to form a stable negative ion [15]. In order to form stable long lived negative ions the electron affinity of the gas must be positive (>0 eV) [10] [15]. The higher the electronegativity of a gas the stronger the force is with which it attracts the electrons. As the electronegativity increases so does the stability of the negative ion.

Direct attachment is the main process to form negative ions in the low electron energy range. The negative ions tend to be more stable than the neutral ions due to a larger electron affinity [20].

- Direct Attachment:

$$e + XY \rightarrow XY^{-} + energy$$

- Dissociative attachment:

$$e + XY \rightarrow X + Y^{-}$$

2.1.3 Scattering Processes

The efficiency of the electron production and depletion processes in gas discharge is largely governed by the electron- particle collisions. During these collisions there is an energy exchange between the electrons and particles and the electrons are scattered. There are two general types of scattering processes: elastic and inelastic scattering. Both elastic and inelastic scattering are responsible for the reduction of the electrons' energies. This reduction of energies strongly affect the probability of a particular reaction occurring on impact [20].

Elastic scattering involves an exchange of kinetic energy between the particles.

- Direct scattering

$$e_{fast} + XY_{slow} \rightarrow XY_{less\ slow} + e_{less\ fast}$$

Inelastic scattering involves the exchange of kinetic energy from the initiating particle to potential energy in the other particle. This potential energy may excite a molecule or form an ion as already discussed.

- Direct scattering

$$e + XY \rightarrow XY^{*} + e$$

- Ion pair formation:

$$e + XY \rightarrow X^{+} + Y^{-} + e$$

- Dissociative scattering:

$$e + XY \rightarrow XY^{-*} \rightarrow X + Y(Y^{*}) + e$$

- Indirect scattering:

$$e + XY \rightarrow XY^{-*} \rightarrow XY + e$$

In both dissociative and indirect scattering the electron is temporarily captured by a molecule to form a negative ion. This is temporary capture is termed negative ion resonance and is considered the most effective way to slow down an electron [20].

When the electron is temporarily captured by a molecule the negative ion formed is in a metastable state. This metastable negative ion decays by auto detachment as shown in the last two scattering reactions. While these metastable states are temporary, they are sufficiently long to slow down the electron, thus, significantly enhancing the probability of scattering in defined energy ranges [15] [20]. In the low energy range (0 to 20 eV), which is the most significant energy range in dielectrics, this resonant process is an efficient slowing down mechanism [10] [15] [20]. Some gases in which low lying NIR states occur are N_2, CO_2, H_2, O_2, and CO [20].

2.1.3.1 Energy Distribution Function

These scattering processes result in a speed distribution related to the temperature and weight of each species of particle. This distribution of speed for a gas in thermal equilibrium is given by the Maxwell-Boltzmann probability distribution [25]:

$$f(s) = 4\pi \left(\frac{m}{2\pi k_B T}\right)^{\frac{3}{2}} s^2 exp\left(-\frac{ms^2}{2k_B T}\right) \tag{4}$$

Where:

$s = speed\ of\ the\ particle$ $(\mathrm{m \cdot s^{-1}})$

$m = mass\ of\ the\ particle$ (g)

$k_B = Boltzmann's\ constant$

$T = temperature$ (K)

Equation (4) can be written in terms of the mean energy (ε) which gives the electron energy distribution function (EEDF):

$$f(\varepsilon) = 2(k_B T)^{\frac{-3}{2}} \sqrt{\frac{\varepsilon}{\pi}} exp\left(\frac{-\varepsilon}{k_B T}\right) \quad (5)$$

Where:

$\varepsilon = energy\ of\ the\ particle$ (eV)

$k_B = Boltzmann's\ constant$

$T = temperature$ (K)

The Maxwell-Boltzmann probability distribution function for electron energy (ε), for different gas temperatures (as obtained using equation (5)) is illustrated in Figure 2. As the gas temperature increases so does the probability of finding an electron at a higher energy and an electron with energy greater than the minimum energy ε_{ion} required for ionisation to occur on collision.

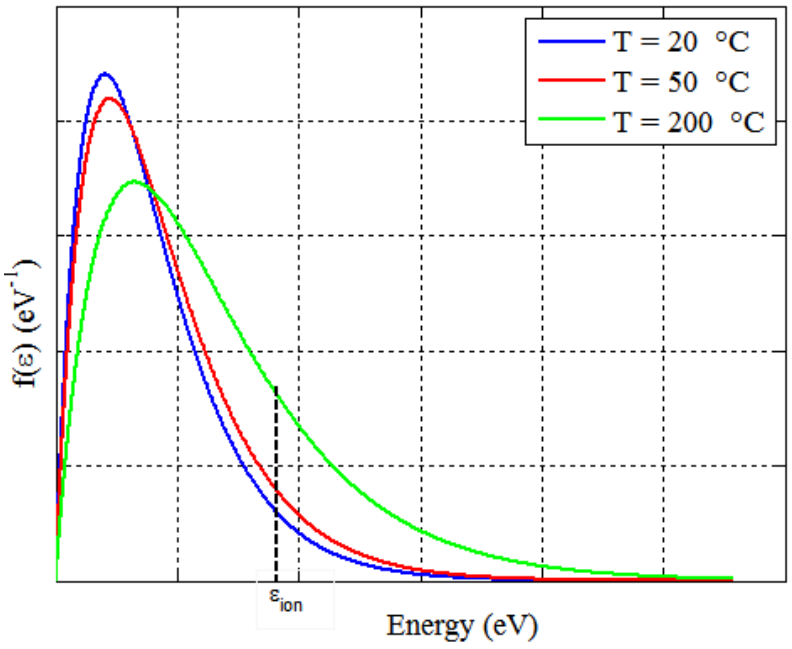

Figure 2: Electron energy distribution function

For illustration purposes equation (5) is normally divided by $\sqrt{\varepsilon}$ and plotted on a semi-logarithmic scale (y) as shown in Figure 3.

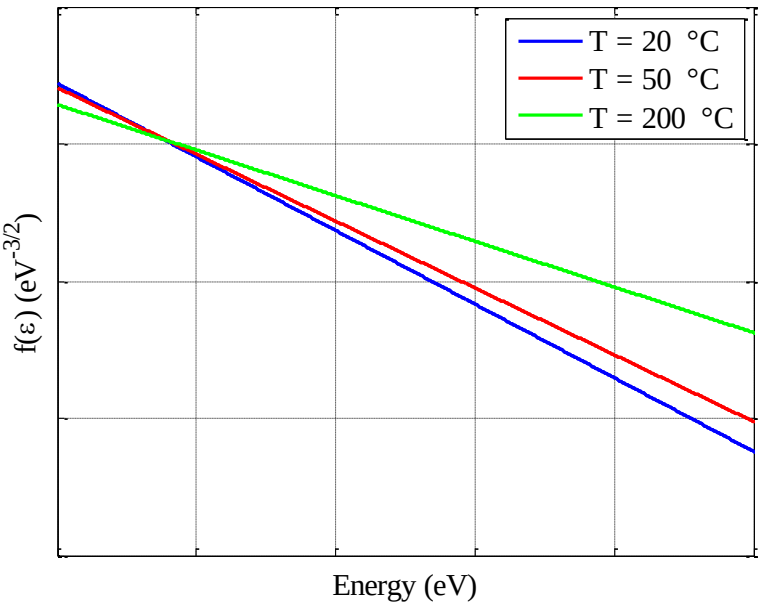

Figure 3: Electron energy distribution function

2.1.3.2 Transport

The application of an electric or magnetic field to a gas has the effect of accelerating a charged particle in the direction of the field through the Lorentz force [17]:

$$\vec{F} = q\left(\vec{E} + \vec{v} \times \vec{B}\right) \tag{6}$$

Where:

$\vec{F} = force\ exerted\ on\ the\ particle$ (N)

$q = charge\ of\ particle$ (C)

$\vec{E} = Electric\ field$ ($\mathrm{V.m^{-1}}$)

$\vec{v} = velocity\ of\ particle$ ($\mathrm{m.s^{-1}}$)

$\vec{B} = magnetic\ field$ (T)

2.1.3.2.1 Mobility

This acceleration of ions and electrons leads to the concept of drift velocity and mobility. Drift velocity is the net movement of the ions and electrons in the direction of the applied field. As a result of this movement the electrons and ions gain energy as given by:

$$\varepsilon = \frac{1}{2}mv_d^2 = \int_0^x e\vec{E}dx \tag{7}$$

Where:

$\varepsilon = energy\ gained$ (eV)

$v_d = drift\ velocity\ of\ particle$ ($\mathrm{m \cdot s^{-1}}$)

$\vec{E} = Electric\ field$ ($\mathrm{V.m^{-1}}$)

$x = distance\ travelled\ by\ particle$ (m)

The mobility, defined as the drift velocity per unit strength of the applied field is given by [25]:

$$\mu = \frac{v_d}{\vec{E}} \tag{8}$$

Where:

$\mu = mobility\ of\ particle$ ($\mathrm{m^2 \cdot V^{-1} \cdot s^{-1}}$)

In essence the mobility/drift velocity describes how easy it is for a charged particle to be moved through the gas by the applied electric field. Lower mobilities lend themselves to a greater dielectric strength as the electrons are unable to gain sufficient energy to aid in the generation of additional free electrons.

2.1.3.2.2 Diffusion

Another important physical quantity for the characterisation of transport of ions and electrons in gases is diffusion. Diffusion is the movement of ions and electrons from regions of high concentrations to regions of lower concentration [25]. The diffusion characterises the speed of the movement of the charge carriers from a high to lower area of concentration. The mobility and the diffusion are linked by the Einstein relation [28]:

$$D = \frac{\mu\, k_B T}{q} \tag{9}$$

Where:

$D = diffusion\ of\ particle$ ($\mathrm{m^2 \cdot s^{-1}}$)

$q = the\ charge\ of\ the\ particle$ (C)

As a result of equation (9) diffusion has a similar effect upon the dielectric strength of a gas as the mobility.

2.2 Breakdown Mechanisms in Gases

Two commonly accepted theories describing breakdown in gases are the Townsend and Streamer mechanism. The Townsend mechanism is based on a sequence of avalanches and is dependent on secondary electron generation processes at the cathode in order for sustained discharge to occur. The Streamer breakdown mechanism is based on an avalanche to streamer transition whereby an initial avalanche becomes sufficiently large that it alters the electric field ahead of it to such an extent that it forms new avalanches ahead of it eventually resulting in the bridging of the gap and breakdown occurring.

2.2.1 The Townsend Mechanism

The Townsend mechanism is based on a lone free electron being accelerated in the direction of the anode by the applied field. During this travel due to impact ionisation additional electrons are freed which in turn are accelerated by the applied field resulting in an exponential increase of electrons as shown in Figure 4.

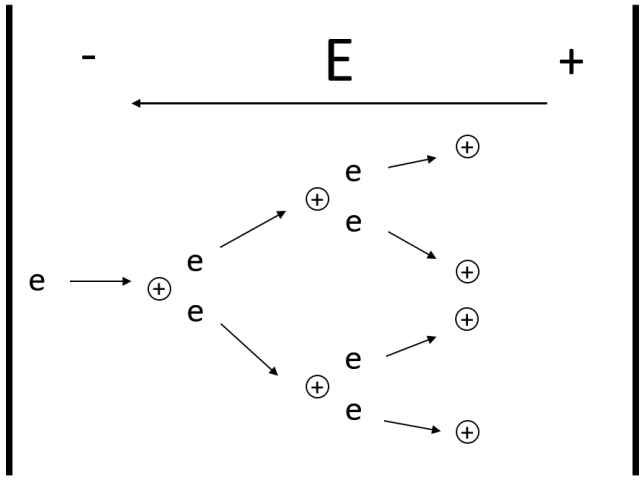

Figure 4: Ionisation by electron collision with gas atoms [29]

2.2.1.1 Townsend's First Ionisation Coefficient

To describe this exponential electron increase or electron avalanche, Townsend's first ionisation coefficient (α) was introduced. Defined as "the number of electrons produced per electron per unit length of travel in the direction of the field" [25]. The number of electrons generated over the distance x from the cathode is given by:

$$n_e = n_0 e^{\alpha x} \tag{10}$$

Where:

$$n_0 = initial\ number\ of\ electrons$$

$$x = distance\ from\ the\ cathode$$

$$\alpha = Townsend's first\ ionisation\ coefficient$$

Equation (10) can be expressed in terms of current by:

$$I = I_0 e^{\alpha x} \tag{11}$$

Where:

$$I_0 = initial\ current\ at\ the\ cathode$$

2.2.1.2 Townsend's Second Ionisation Coefficient

Measurements showed that at higher voltages the increase in current was more rapid than described by equation (11). This led to the belief that there must be a secondary affect contributing to the production of electrons. An electron avalanche having travelled distance x generates a total of $n_0(e^{\alpha x} - 1)$ positive ions. Over the distance to the cathode the positive ions build up sufficient kinetic energy to release electrons on impact with the cathode. The number of electrons released by the impact of these positive ions is given by:

$$n_0' = \gamma n_0(e^{\alpha x} - 1) \tag{12}$$

Where

$$\gamma = Townsend' second\ ionisation\ coefficient$$

$$n_0' = Number\ of\ secondary\ electrons$$

Townsends second ionisation coefficient is defined as the number of electrons produced per incident positive ion. Combining the number of primary and secondary electrons released gives the total number of electrons n reaching the anode as [21]:

$$n = (\mathrm{n}_0 + \mathrm{n}_0{}')e^{\alpha x} \tag{13}$$

This simplifies to:

$$n = \frac{n_0 e^{\alpha x}}{1 - \gamma(e^{\alpha x} - 1)} \tag{14}$$

Equation (14) can be expressed in terms of current by:

$$I = \frac{I_0 e^{\alpha x}}{1 - \gamma(e^{\alpha x} - 1)} \tag{15}$$

Therefore, as the voltage is increased the current increases according to Equation (15). The electrical discharge transitions from a non-sustained to self-sustained discharge when the current tends to infinity. This occurs when the denominator in equation (15) tends to zero.

Taking into account the attachment coefficient (η) this gives the Townsend criterion for spark breakdown:

$$\gamma\left(e^{(\alpha-\eta)x}-1\right)=1 \tag{16}$$

If equation (16) is greater than one, the discharge will grow rapidly leading to a self-sustained discharge. If equation (16) is less than one the discharge will be a non-sustained discharge.

2.2.2 The Streamer Mechanism

According to the Townsend mechanism of breakdown, current growth is due to electron production and depletion processes only; however, in practice the breakdown voltage is dependent on gas pressure, gap distance and gap geometry. In addition, formative time lags of several microseconds were expected. However, experimental observation showed that breakdown occurred much faster [25] [30] [31]. The failure of the Townsend mechanism to account for these phenomena led Raether, Loeb and Meek to (independently) propose the Streamer theory [21] [29].

Raether, Loeb and Meek proposed that breakdown occurs as the result of a single avalanche whose space charge is sufficiently large to enhance the applied electric field ahead of it to such an extent that secondary avalanches form, leading to the eventual bridging of the gap and breakdown [21] [29].

Figure 5 shows the effect of the avalanches' progression on the electric field. Field enhancement is observed between the head and the anode, and between the tail and the cathode. The field between the head and the tail is reduced. Studies on the effect of space charge show field distortion becomes noticeable with a charge carrier number $n > 10^6$. If the charge density in the avalanche approaches $n = 10^8$ the space charge field and the applied field will have the same order of magnitude, leading to the initiation of the streamer [25] [30].

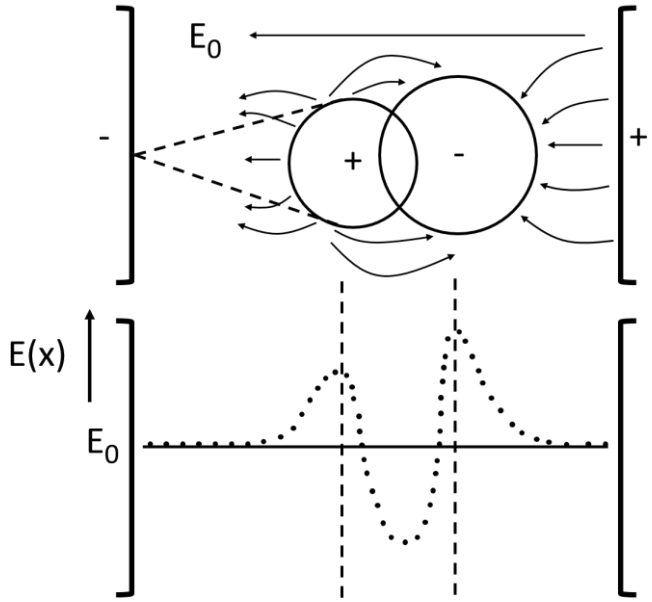

Figure 5: Field distortion in a gap caused by space charge of electron avalanche [25]

It has been observed from measurements that the transition from avalanche to streamer generally occurs when the charge in the avalanche head reaches a critical concentration given by [25]:

$$n_0 e^{|\alpha x_c|} \approx 10^8 \quad \text{or} \quad \alpha x_c \approx 18 - 20 \tag{17}$$

Where:

$x_c = length\ of\ the\ avalanche\ path\ when\ critical\ concentration\ is\ reached$

If x_c is larger than the gap length the initiation of a streamer is unlikely [25]. When the avalanche reaches its critical size, the field enhancement caused by the space charge leads to intense ionisation and excitation of the particles in front of the avalanche head [25].

Recombination of electrons and positive ions generates photons (as discussed in section 2.1.1.1.2) which generate secondary electrons through photo-ionisation. Under the influence of the enhanced electric field these electrons develop into secondary avalanches as shown in Figure 6. The high mobility of the photons leads to the rapid development of a conduction channel.

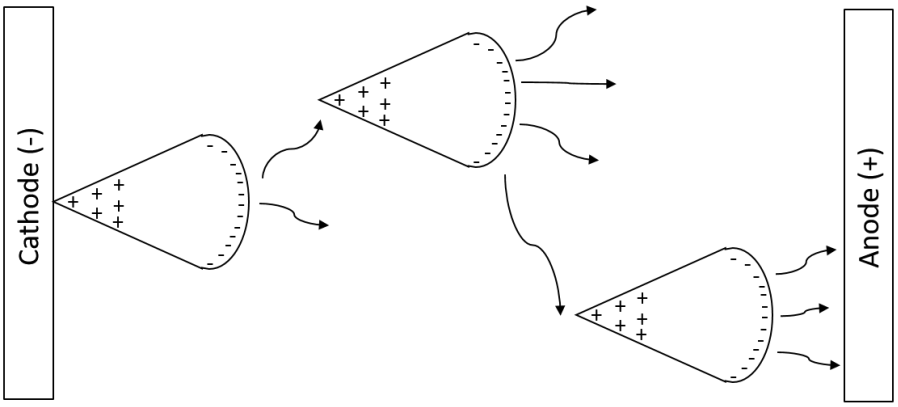

Figure 6: Photo-ionisation causing secondary electron avalanches [21]

From experimental investigation Raether developed an equation for the streamer spark criterion:

$$\alpha x_c = 17.7 + \ln(x_c) + \ln\left(\frac{E_r}{E}\right) \tag{18}$$

Where:

$E_r = the\ space\ charge\ field$ $(\mathrm{V \cdot m^{-1}})$

$E = the\ applied\ field$ $(\mathrm{V \cdot m^{-1}})$

The resultant field at the head of the avalanche is enhanced to $(E_r + E)$, while the field between the avalanche head and tail is reduced to $(E - E_r)$. The transition from avalanche to streamer occurs as the magnitude of the space charge field tends to that of the applied field. Therefore equation (18) becomes:

$$\alpha x_c = 17.7 + \ln(x_c) \tag{19}$$

In a uniform field the minimum breakdown by Streamer mechanism occurs when the avalanche has just crossed the gap (i.e. $x_c = d$) [25]. This results in equation (19) becoming:

$$\alpha d = 17.7 + \ln(d) \tag{20}$$

Where:

$d = gap\ length$

Thus $\alpha x_c = d$ gives the smallest value of α to produce streamer breakdown. Thus when including the attachment coefficient the streamer criterion becomes [25]:

$$\bar{\alpha} d = 18 - 20 \tag{21}$$

2.3 Electrode Effects

Outside of the nature of the gas, its number density and the applied voltage the electrode has the most significant impact on the breakdown of a gaseous dielectric [32] [33]. In particular, the breakdown voltage of a gas is affected by the following properties of the electrode:

- Electrode material: the work function of an electrode is determined by the material. The work function affects the processes of photoelectric emission (section 2.1.1.4) and electron detachment due to collision of ions (section 2.1.1.3) with electrodes.
- Electrode surface roughness: surface roughness creates localized microscopic regions with electric field intensities far higher than the average. Depending on the gas pressures this enhanced electric field strength may result in a reduction of the breakdown voltage [33] [34] [35]. Increasing pressures tends to result in surface roughness playing a stronger role in the reduction of the breakdown voltage of the gas [36].
- Electrode area: an increase in surface area increases the probability of photoelectric emission and collision of ions with the electrodes. This results in a decrease in breakdown voltage as the electrode surface area is increased.
- Electrode separation: the breakdown in compressed gases generally decreases with an increasing gap distance, especially at high pressure and fields, which can result in a saturation effect on the breakdown voltage [37].
- Electrode geometry: the electrode geometry has the most significant impact on the breakdown voltage in a gas as the electrodes determine whether the electric field is uniform or not. The uniformity of the field affects the occurrence of stressed points and hence the mechanism by which breakdown occurs. The more non-uniform the geometry the lower the breakdown voltage.

2.4 Tailoring of Gaseous Dielectrics

A gaseous mixture may be tailored for a specific application by altering the component gases used and varying their proportions according to their individual properties [1] [13] [20]. A gas mixture may be tailored in order to [1]:

- Decrease the boiling point (through the addition of gases with low boiling points)
- Decrease cost (through the addition of cheaper gases)
- Decrease GWP (through the addition of low GWP gases)
- Improve non-uniform field behaviour
- Increase dielectric strength

Christophorou et al found that the dielectric strength of a gas could be optimised by controlling the number of free electrons and their energies. To control the number of free electrons in a gas the attachment cross-section (see section 2.4.1) of the gas should be as large as possible over as wide an energy range as possible in order to facilitate free electron removal. At the same time the ionisation cross-section of the gas should be as small as possible over as narrow an energy range as possible in order to reduce free electron generation. By reducing the free electron energies the EEDF (see section 2.1.3.1) is reduced which increases the attachment cross-section and decreases the ionisation cross-section [10] [13] [15] [20].

In particular Christophorou et al showed that to optimise a dielectric gas equation (22) should be maximised and equation (23) should be minimised.

$$\int_0^\infty \sigma_a(\varepsilon) f(\varepsilon, E/N) d\varepsilon \tag{22}$$

$$\int_I^\infty \sigma_i(\varepsilon) f(\varepsilon, E/N) d\varepsilon \tag{23}$$

Where:

$\sigma_a(\varepsilon) = \ the\ attachment\ cross\ section$

$\sigma_i(\varepsilon) = the\ ionisation\ cross\ section$

$f(\varepsilon, E/N) = \ the\ electron\ energy\ \ distribution\ function$

$E = \ the\ electric\ field\ strength$

$N = \ the\ gas\ number\ density$

Through equations (22) and (23) a gaseous mixture may be tailored to achieve significant synergistic effects [13]. Typically these synergistic effects are observed when an electronegative gas and an electron-retarding/buffer gas are combined [13]. In these mixtures the buffer gas scatters the electrons, which reduces the EEDF of the mixture while the electronegative gas efficiently removes the electrons. Examples of this synergistic effect are observed in SF_6-N_2 and SF_6-CO_2 mixtures.

2.4.1 Collisional Cross Sections

Due to their significantly lighter mass electrons are most affected by the Lorentz force and thus may gain sufficient kinetic energy to excite or ionise a neutral molecule upon inelastic collision with it.

The collision between two particles (electron-neutral) is described using a fundamental property called the collision cross section [38]. The collisional reactions of a gas are based on a probability phenomenon related to the energy of the electron and a collisional cross sectional area (σ) for each type of reaction [25]. The collisional cross section is defined as the cross sectional area for interception relating the area of the colliding particle to the area of the struck particle $\sigma = \pi(r_1 + r_2)^2$ [25]. The cross section for a gas is highly dependent on the incident electron energy.

2.4.1.1 Electron Collisions in Sulphur Hexafluoride

Collisional cross sections for SF_6, are illustrated in Figure 7. The cross sections are obtained from the LXCat database and are used for the modelling [39]. Figure 7 illustrates that for any given electron energy there are a number of reactions that could take place, with attachment being the most likely reaction for energies below 0.1 eV and a momentum collision for higher electron energies.

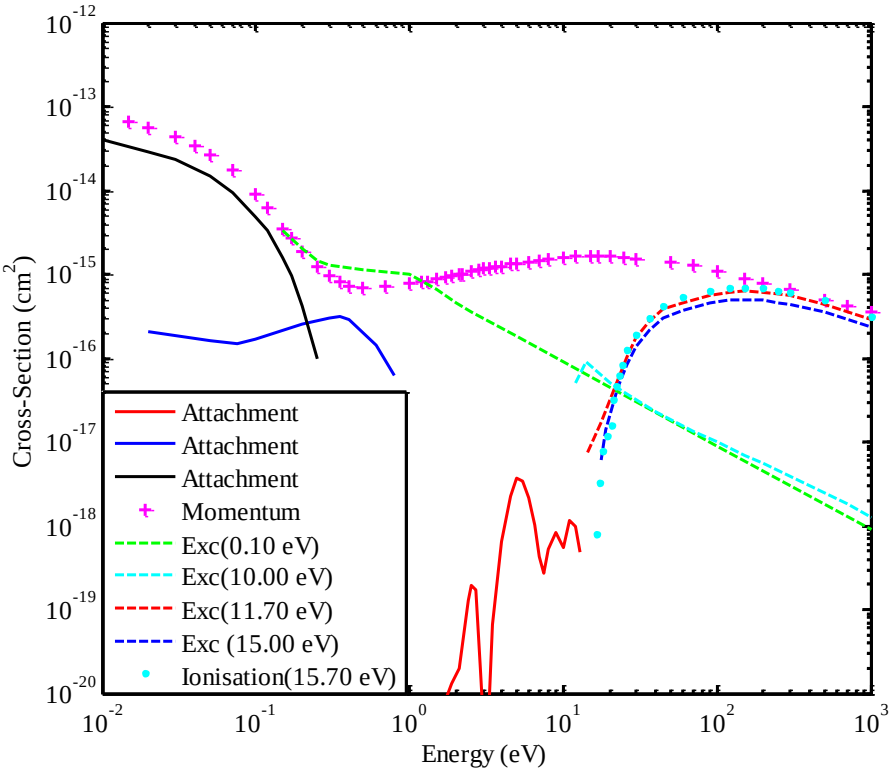

Figure 7: Electron collision cross sections in SF6 [39]

The strong attachment cross section of SF_6 for energies below 1 eV plays an important role in the dielectric strength of SF_6 as it inhibits the initiation and growth of electrical discharges [40]. While only a small fraction of the electron energies will lie below 1 eV the large attachment cross section quickly removes all the free electrons in this range: forming stable negative ions which do not participate in further ionisation processes [10] [15] [18]. With the removal of the low energy electrons (the slow electrons) the EEDF has to recover its functional form, in order keep its steady state unchanged, by feeding the depleted low-energy portion from the higher energies [10] [15] [20]. This recovery of its functional form occurs on a time scale much shorter than the time to breakdown [10] [15] [20]. The "new" low energy electrons will again be removed due to the large

attachment cross section in SF_6 and the EEDF will have to recover its functional form again [10] [15]. This process will repeat, thus removing free electrons.

This ability of SF_6 to effectively remove low energy/slow electrons along with an ionisation cross section at high electron energies only, results in SF_6 being an excellent dielectric [10] [15].

2.4.1.2 Electron Collisions in Nitrogen

Collisional cross sections (excluding rotational and vibrational) for N_2 are illustrated in Figure 8. The cross sections are obtained from the LXCat database [39].

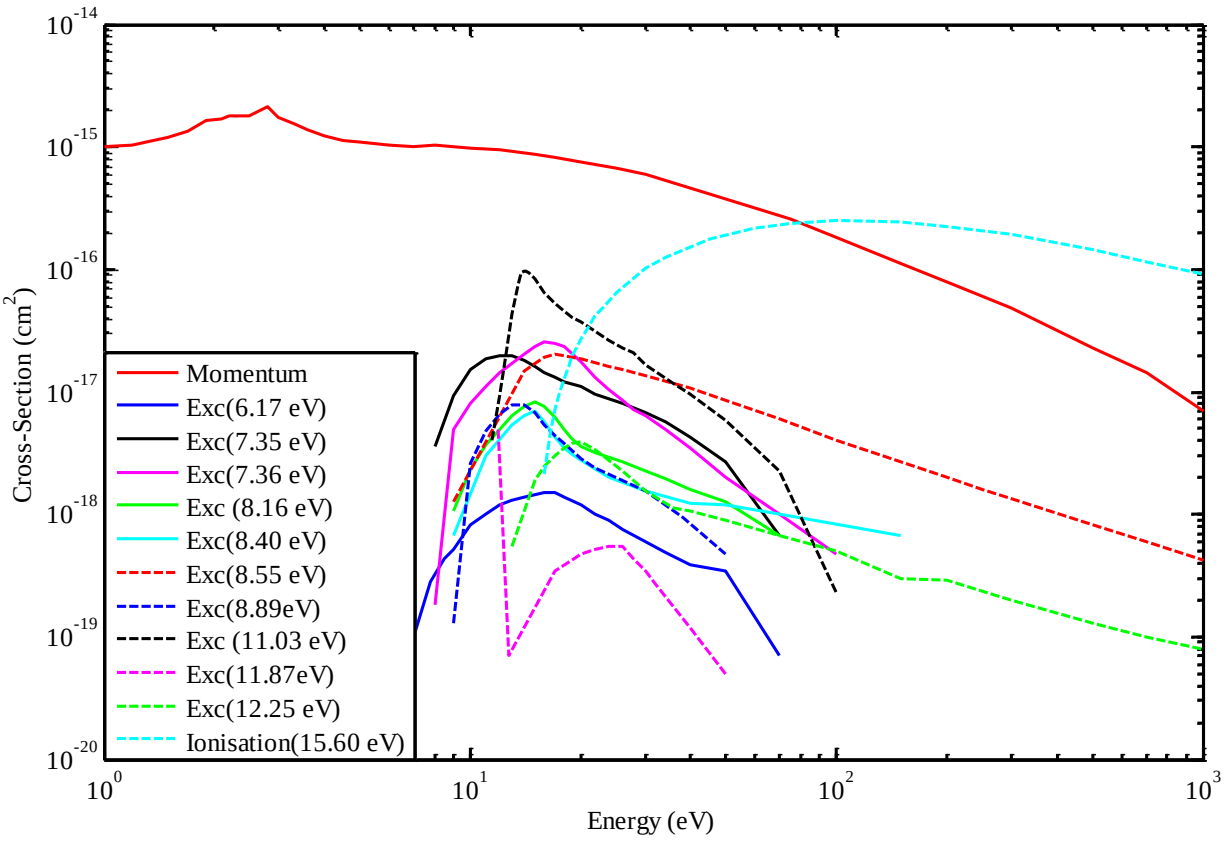

Figure 8: Electron collision cross sections in N_2 [39]

Figure 8 illustrates that for low electron energies a momentum collision is the most likely reaction with ionisation collisions becoming more probable as the electron energies increase. The multiple excited states of N_2 act as temporary energy sinks as they retard the acceleration of electrons therefore keep the electron energies low. As a result even though N_2 has no attachment cross section its dielectric strength is very good [10].

2.4.1.3 Electron Collisions in Carbon Dioxide

Collisional cross sections for CO_2 are illustrated in Figure 9. The cross sections are obtained from the LXCat database [39]. Figure 9 illustrates that just like N_2, CO_2 has momentum as the most likely reaction for low electron energies, with ionisation collision beginning to dominate as the electron energy is increased. However, CO_2 has fewer excited states and an attachment cross-section.

The multiple excited states of CO_2 retard the acceleration of electrons while the attachment enables the removal of electrons. As a result, CO_2 is considered a good insulator.

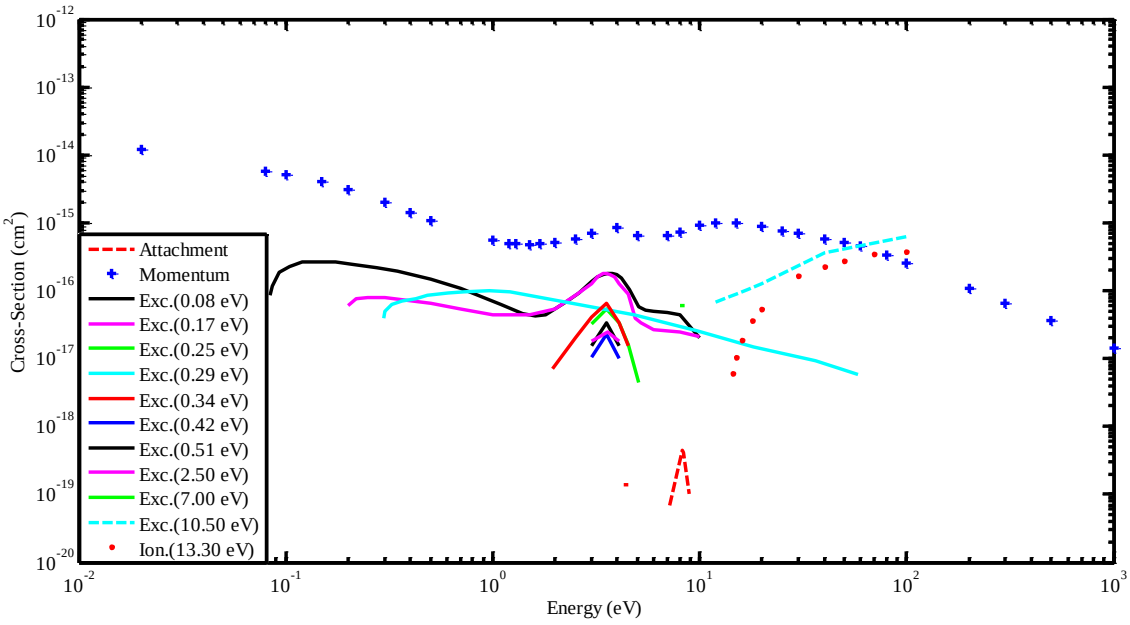

Figure 9: Electron collision cross sections in CO_2 [39]

2.4.2 Impulse Breakdown of Gases

The impulse breakdown of gases occurs with a characteristic rise time that is on the same order of magnitude as the fundamental processes in gas discharge [19]. As a result, unlike the DC and AC breakdown voltages whose characteristic rise times are much longer than the times constant of the fundamental processes of gas discharge, the impulse breakdown voltage is a stochastic time dependant quantity [19].

The synergy effect in a mixture occurs as the electrons are slowed down by the buffer gas and removed by the electronegative gas. As this occurs the EEDF of the gas needs to recover its form by feeding in fast electrons to lower energies. As these processes of

electron energy reduction and electron removal are fundamental processes in gas discharge the synergy effect occurs with the time characteristic of the fundamental processes. As a result a difference of efficiency is expected between the discharges caused by DC and AC voltages compared to impulse discharge [18] [19].

Figure 10 shows the impulse breakdown divided into four time intervals [19]. T_0 is the time upon which the impulse voltage reaches the value of DC breakdown voltage for the electrode configuration. T_s is the statistical time which occurs after T_0 until the appearance of an initiary electron. T_l is the avalanche process time during which the first avalanche is turned into a full self-sustaining discharge. T_f is the time required for the formation of the channel [18]. The sum of the time intervals is called the breakdown time and of the four intervals the statistical time contributes most to stochastic nature of the impulse breakdown as the statistical time lag for the initiary electron to appear can vary between milliseconds and seconds [18] [32].

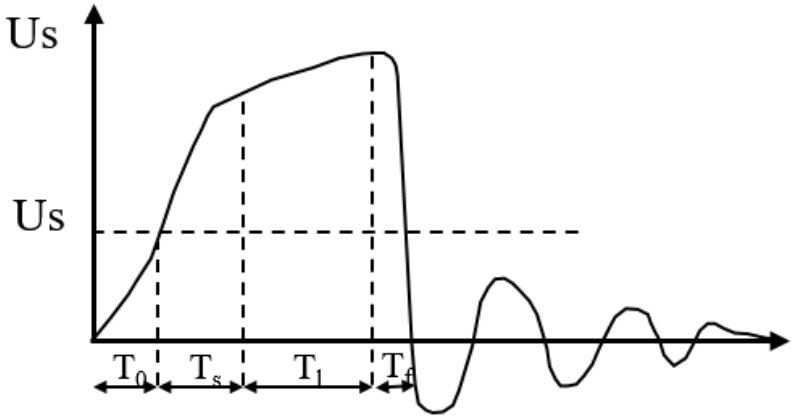

Figure 10: Time dependence of impulse breakdown voltage in gases [18]

2.5 Boltzmann Equation, EEDF and Coefficients

Given the fundamental collision cross-section data the Boltzmann equation may be used to solve for the EEDF (see section 2.1.3.1) and electron coefficients (transport, rate and Townsend) of a given discharge.

The Boltzmann equation is given by [41]:

$$\frac{\partial f}{\partial t} = \vec{v}.\nabla f - \frac{q}{m}\vec{E}.\nabla_v f = \left(\frac{\partial f}{\partial t}\right)_{collision} \tag{24}$$

Where:

$\vec{v} = velocity\ of\ particle$ $(m \cdot s^{-1})$

$q = charge\ of\ particle$ (C)

$m = mass\ of\ the\ electron$ (g)

$\vec{E} = Electric\ field$ $(V.m^{-1})$

2.5.1 Bolsig+

Developed by Hagelaar and Pitchford [41] , Bolsig+ is a Boltzmann equation solver that is used to calculate the EEDF and electron coefficients, required as inputs for a fluid model (section 3.1), by providing steady state solutions of the Boltzmann equation in a uniform electric field.

Using the cross sections from the LXCat database [39] the input parameters for Bolsig+ were:

Gas Temperature (K):	293
Ionisation degree:	10^{-5}
Electron density (m^{-3}):	10^{20}

Electron-electron collisions were included. Hagelaar and Pitchford [41] show that the inclusion of the electron-electron collisions results in the EEDF tending towards a Maxwellian distribution function with their influence being greatest for an ionisation degree greater than 10^{-6}. Hagelaar and Pitchford also believe that the most important consequence of the electron-electron collision for fluid models is that they increase the rate coefficients of the ionisation and excitation coefficients by repopulating the tail of

the EEDF. However, the rate coefficients are only increased at low electron energies due to the cross sections for electron-electron collisions dropping off with increasing electron energy. As a result for discharges where the ionisation degree is low or the mean electron energy is high the influence of the electron-electron collision may be ignored for simplicity sake [41]. Breakdown in gaseous insulation tends to have electrons with high energy so the electron-electron collisions may be ignored. Further information on the operation and behaviour of Bolsig+ can be found in [41].

2.5.1.1 The Mean Energy and Electron Energy Distribution Function

Figure 11 shows the mean energy (ε) as a function of SF_6 content for SF_6-N_2 and SF_6-CO_2 mixtures for an E/N of 500 Td obtained using Bolsig+. The mean energy is a summary of the EEDF under specific conditions.

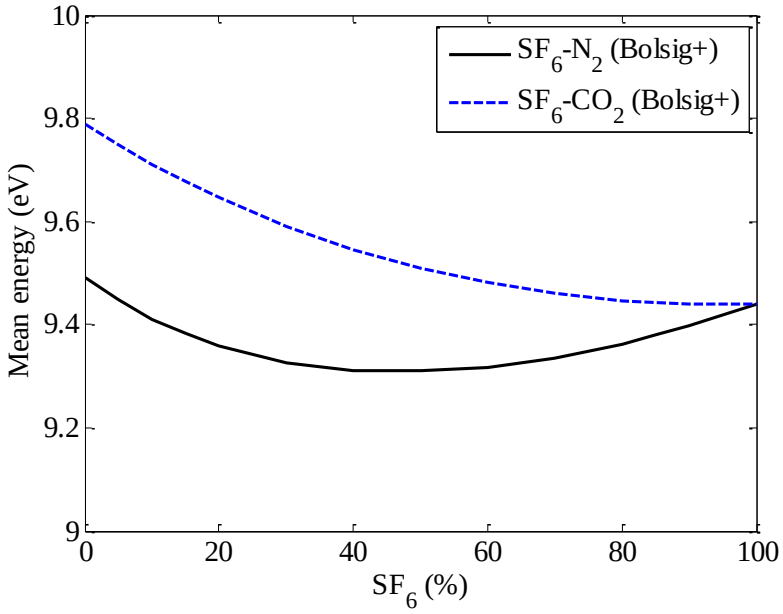

Figure 11: Mean electron energy for SF_6-N_2/CO_2 calculated using Bolsig+

The mean energy of the SF_6-N_2 has a trend of decreasing with increasing SF_6 content. However, there appears to be a minimum mean energy at 50% SF_6 content, after which increasing SF_6 results in a slight rise in mean energy. The mean energy of the SF_6-CO_2 mixture decreases with increasing SF_6 content with the lowest mean energy occurring at 100% SF_6 content. The changes in the mean energy of the mixtures as the SF_6 content increases occurs due to the EEDF altering.

Figure 12 shows the effect increasing the SF_6 content in a SF_6-N_2 mixture has on the EEDF. It can be seen that for the E/N of 500 Td the increase of SF_6 content alters the

EEDF by shifting it to lower energies. The increase of SF_6 content also results in the decrease of the EEDF in the vicinity of the origin of energy space $\varepsilon = 0$ [42]. This net decrease in the EEDF as the SF_6 content is increased results in a net decrease of the mean energy. The minimum mean energy observed in Figure 11 is due to what occurs in the EEDF (Figure 12) between 5 eV and 22 eV. Between these two points the EEDF increases as the SF_6 content increases. The point at which the increasing portion of the EEDF balances the decreasing portion of the EEDF is observed as the minimum mean energy in Figure 11.

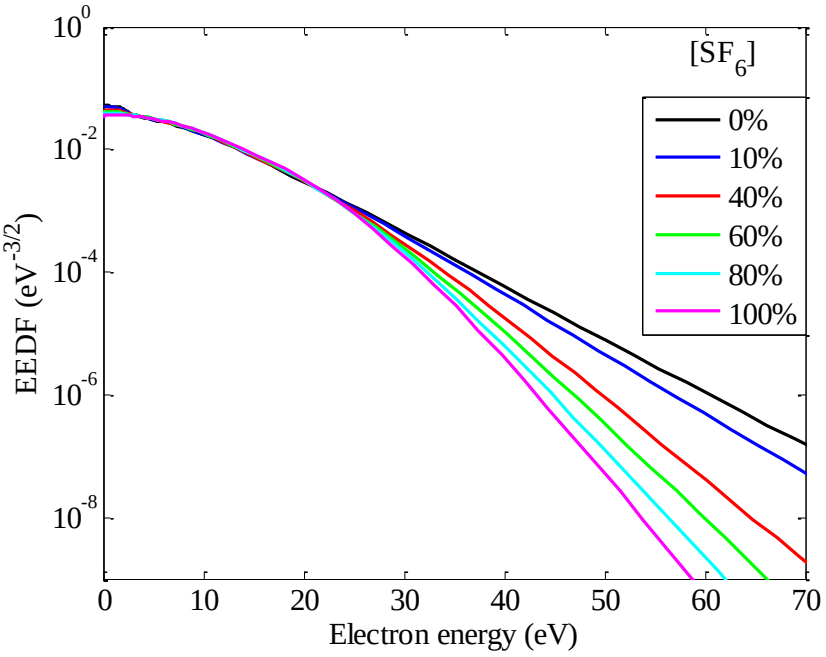

Figure 12: EEDF for SF_6-N_2 at 500 Td calculated using Bolsig+

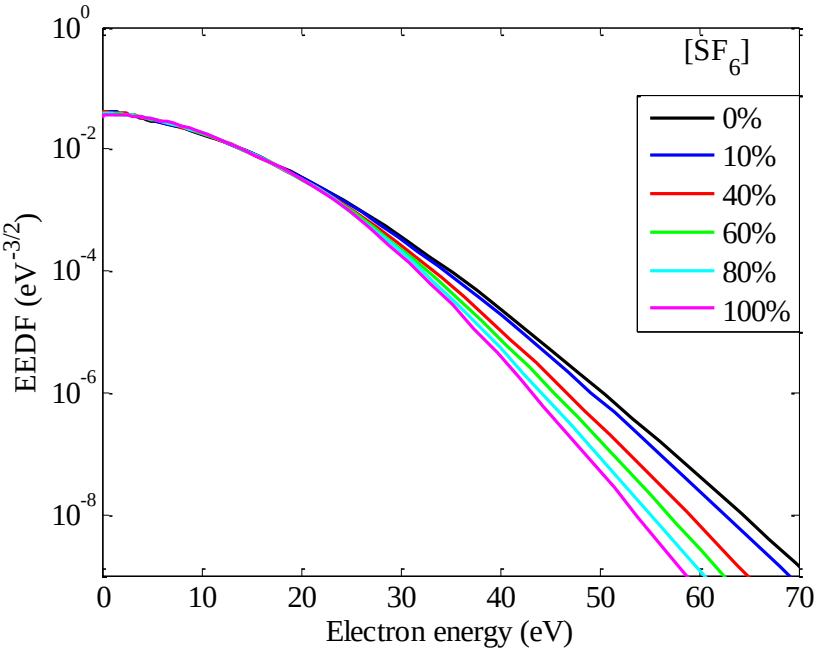

Figure 13: EEDF for SF_6-CO_2 at 500 Td calculated using Bolsig+

The addition of SF_6 in the SF_6-CO_2 mixture has the effect of decreasing the EEDF. While the EEDF differs imperceptibly near ε = 0, it shifts to lower energies as shown in Figure 13. This reduction of the EEDF results in a decreasing mean energy as the SF_6 content increases.

2.5.1.2 Townsend Coefficients

The Townsend coefficients can be determined for each collision type by the integral relationship of the particle energy, the cross-section and the electron distribution using equation (25) [17] [41]:

$$\frac{\alpha_k}{N} = \sqrt{\frac{2q}{m}} \frac{\int_0^\infty \varepsilon \sigma_k f d\varepsilon}{\mu E} \tag{25}$$

Where:

$$\sigma_k = Collisional\ cross-section\ of\ collision\ type\ k\ (\mathrm{cm}^2)$$

Figure 14 validates the use of Bolsig+ for determining the Townsend coefficients by illustrating the close correlation between Bolsig+'s calculated effective ionisation coefficient and experimentally obtained values for pure SF_6, N_2 and CO_2 from Christophorou et al [9], Qiu et al [43], de Urquijo et al [44] and Hernández-Ávila et al

[45]. Note that Bolsig+ includes only collisional data in the calculation of the cross sections while measured data would include other influences [17].

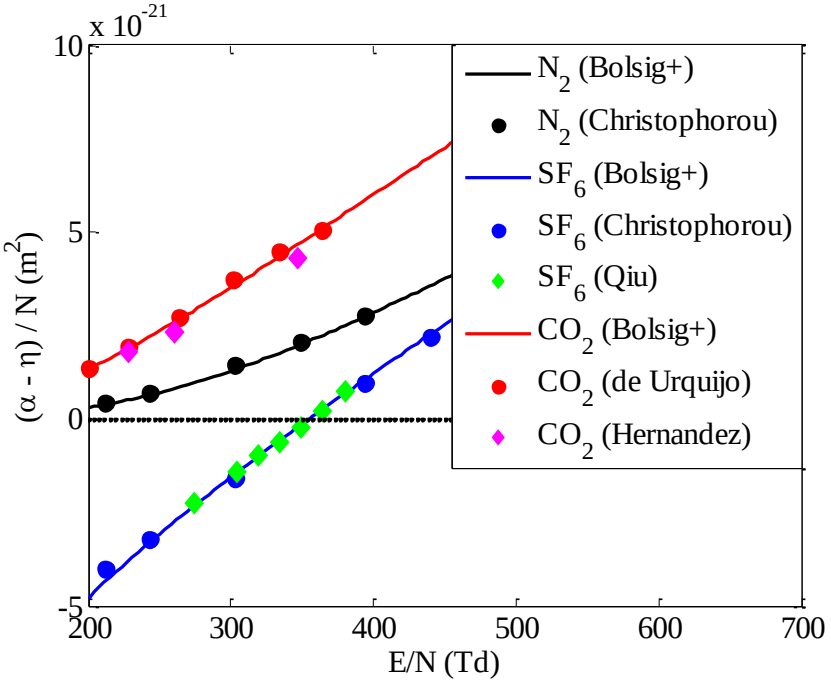

Figure 14: Effective ionisation coefficient as a function of E/N for SF_6, N_2 and CO_2

The number density reduced effective ionisation coefficients (α-η)/N are calculated for 0%, 10%, 40%, 60%, 80% and 100% content of SF_6 in SF_6-N_2 and SF_6-CO_2 mixtures. The results, as a function of the reduced field strength, are displayed in Figure 15 and Figure 16. Both figures illustrate that the effective ionisation coefficient increases with increasing electric field strength. The increase of the reduced electric field strength favours ionisation as the ionisation cross section is greatest and the attachment cross section is lowest at high electric field strengths. It can also be observed that for a given electric field strength the effective ionisation coefficient decreases as the SF_6 content increases for both the SF_6-N_2 and SF_6-CO_2 mixtures. This reduction in the effective ionisation coefficient is due to the increasing electronegativity of the mixtures resulting in larger attachment cross sections. In addition the increase of the SF_6 content in the SF_6-N_2 and SF_6-CO_2 mixtures causes the EEDF to shift to lower energies, as shown in Figure 12 and Figure 13, resulting in a reduction of the mean electron energy. Due to the electron attachment cross section being greatest at low energies this reduction in the EEDF results in a lower effective ionisation coefficient.

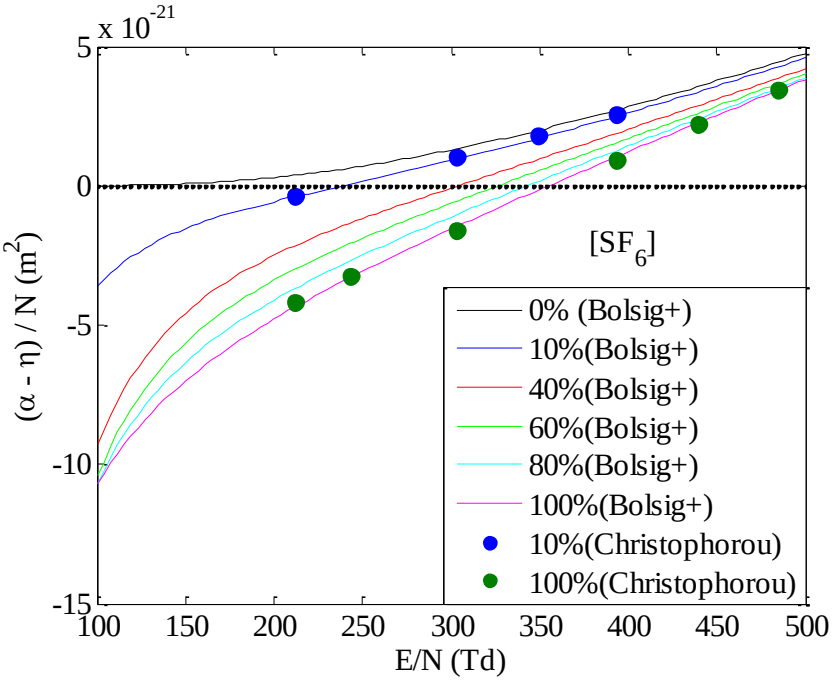

Figure 15: Effective ionisation coefficient in SF_6-N_2 mixtures

Comparison of Figure 15 and Figure 16 show a marked difference in the SF_6-N_2/CO_2 mixture behaviour at high E/N values. The effective ionisation coefficients for the SF_6-N_2 mixtures converge while for the SF_6-CO_2 mixtures do not.

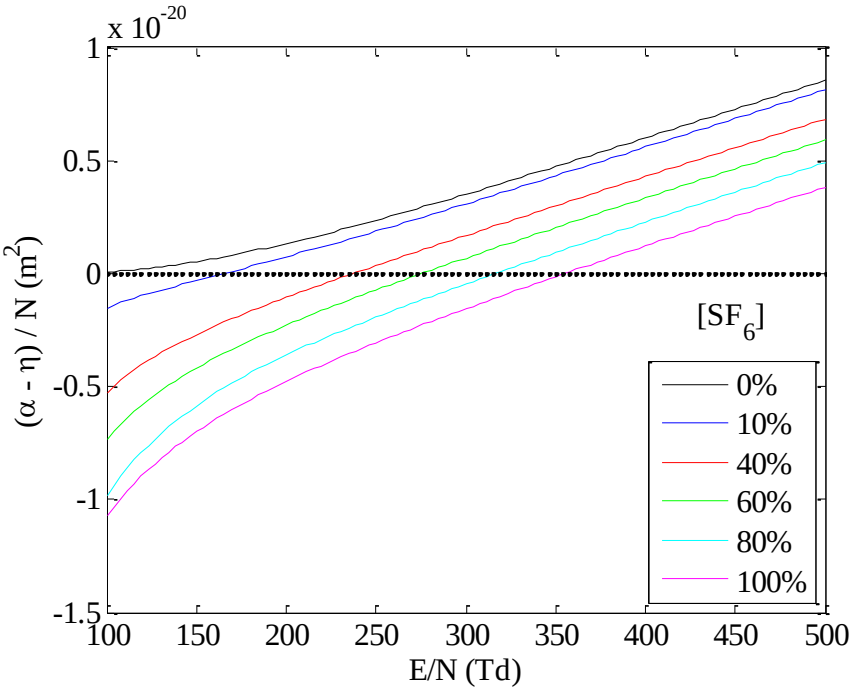

Figure 16: Effective ionisation coefficient for SF_6-CO_2 mixtures

This difference may be attributed to the electron energies at which the electron scattering cross sections for N_2 and CO_2 peak. The total electron scattering cross sections for N_2 and CO_2 are shown in Figure 23 and Figure 24. The electron scattering cross-section for N_2 peaks between 2 eV and 3 eV while for CO_2 the electron scattering cross section peaks below 0.1 eV, at 4 eV and at 40 eV. The numerous scattering peaks of N_2 at low energies efficiently slow down the electrons at low electric fields. At higher electric fields the electrons are not slowed down by the N_2 so its role in the effective ionisation coefficients is reduced resulting in the effective ionisation coefficient tending to that of pure SF_6. The scattering peaks of the CO_2 at higher energies enable the reduction of electron speed at higher electric fields so the CO_2 continues to play a significant role in determining the effective ionisation coefficient.

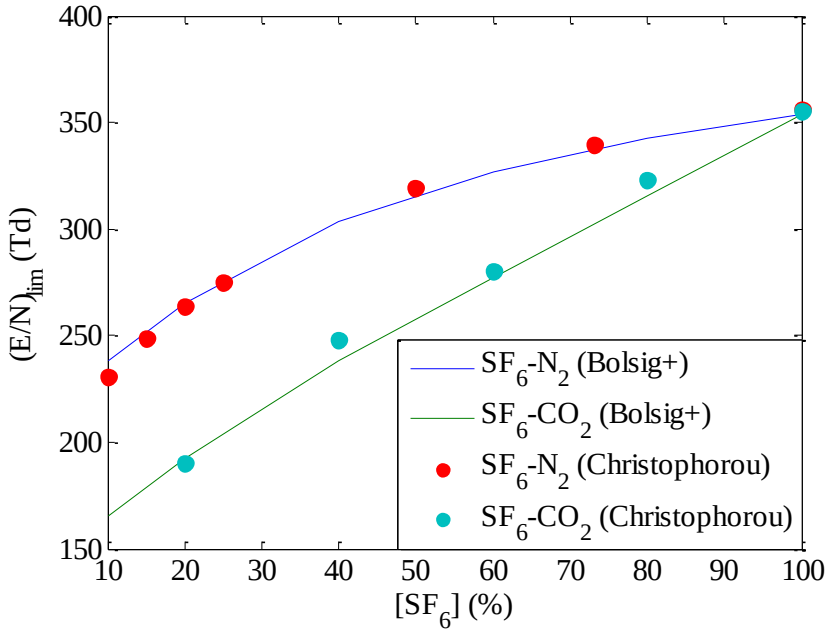

Figure 17: Critical field strength for SF_6-N_2 and SF_6-CO_2

The critical electrical field strength $(E/N)_{lim}$ for the SF_6-N_2 and SF_6-CO_2 mixtures compared with results from Christophorou and van Brunt [9] are plotted in Figure 17 as a function of the SF_6 content. It can be seen that the critical field strengths obtained from Bolsig+ are in good agreement with the experimental data.

2.5.1.3 Drift Velocity

The mobility of the electrons is described by the integral relationship between the energy and all collisional cross sections as follows [41] [17]:

$$\frac{\mu}{N} = -\frac{1}{3}\sqrt{\frac{2q}{m}}\int_0^\infty \frac{\varepsilon}{\sigma_m}\frac{\partial f}{\partial t}d\varepsilon \tag{26}$$

Where:

$\mu = mobility\ of\ electron$ ($\mathrm{cm^2.V^{-1}.s^{-1}}$)

$N = number\ density\ of\ neutral\ molecules$ ($\mathrm{cm^{-3}}$)

$\varepsilon = energy\ of\ electron$ (eV)

$\sigma_m = total\ collisional\ cross\ section$ ($\mathrm{cm^2}$)

The drift velocity (v_d) of electrons for a given electric field may be determined from the mobility [25]:

$$\vec{v}_d = \mu\vec{E} \tag{27}$$

Figure 18 compares the electron drift velocity as a function of the number density reduced electric field obtained from Bolsig+ to experimental values obtained from de Urquijo [46], Hendrick [47] and Vivaldini et al [48] for N_2.

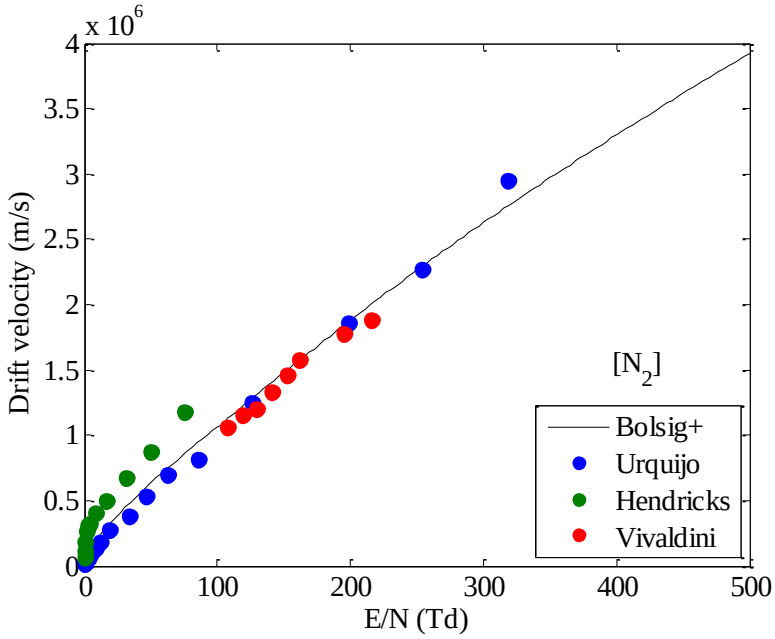

Figure 18: Drift velocity as a function of E/N for N_2

Figure 19 compares the calculated results of the drift velocity to experimental results from Liu et al [49], de Urquijo et al [44], Hernández-Ávila et al [45], Yoshinga et al [50](cited in [49]) and Sierra et al [51] for CO_2. The calculated electron drift velocity as a function of the number density reduced electric field for SF_6 are compared to experimental results from Christophorou [9], Harris et al [52] and Aschwanden [53] (cited in [54]) in Figure 20.

The close correlation between the calculated results from Bolsig + and published experimental results as shown in Figure 18, Figure 19 and Figure 20 validating the use of Bolsig+ as a solver for the transport coefficients.

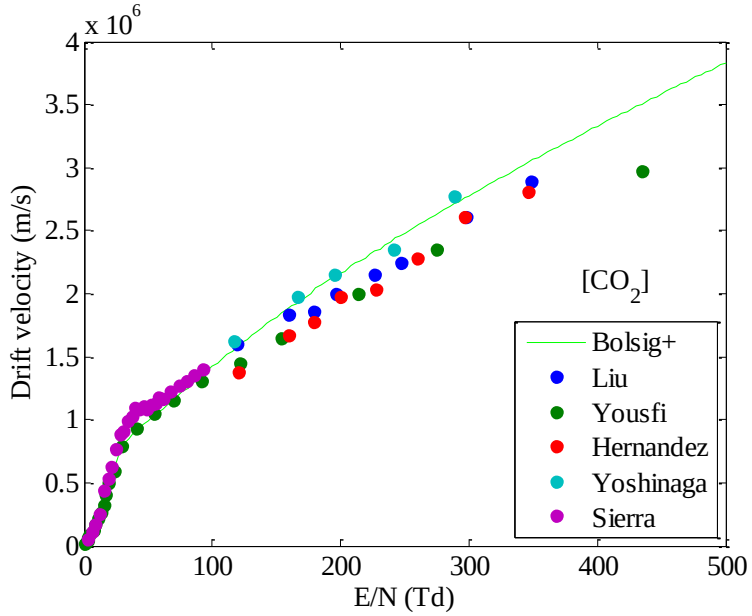

Figure 19: Drift velocity as a function of E/N for CO_2

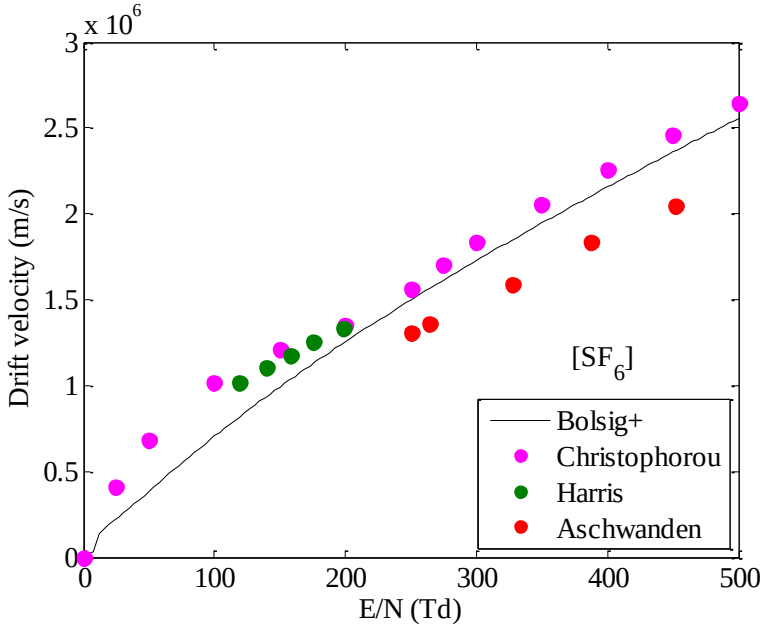

Figure 20: Drift velocity as a function of E/N for SF_6

The electron drift velocity as a function of the reduced field for SF_6-N_2 and SF_6-CO_2 mixtures (obtained using Bolsig+) are illustrated in Figure 21 and Figure 22. Both figures show that as the electric field strength increases (E/N) so does the drift velocity. With increasing SF_6 content the drift velocity is lower in the SF_6-N_2 and SF_6-CO_2 mixtures with the reduction of drift velocities becoming more pronounced at higher electric field strengths.

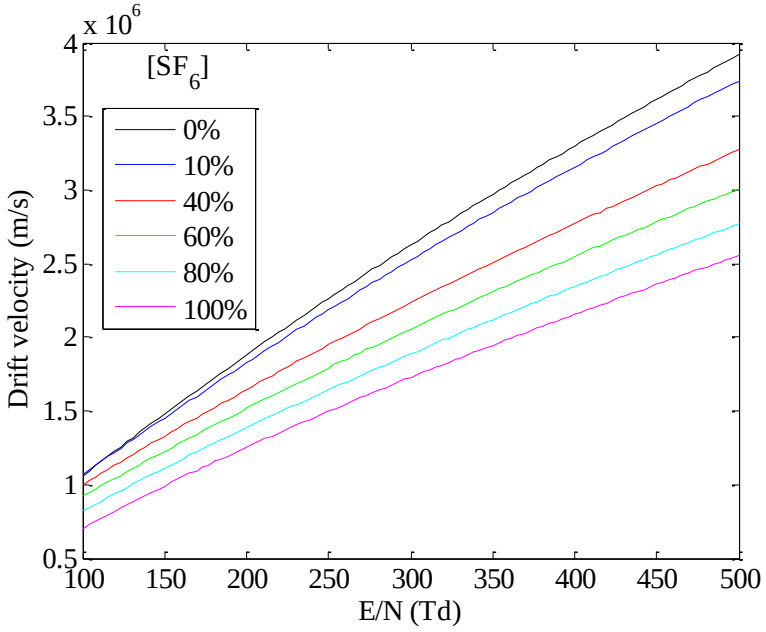

Figure 21: Drift velocity in SF_6-N_2 mixtures calculated using Bolsig+

It is also of interest that at lower electric field strengths the SF_6-N_2 mixtures tend to exhibit lower drift velocities than the SF_6-CO_2 mixture while the opposite is true at higher electric fields.

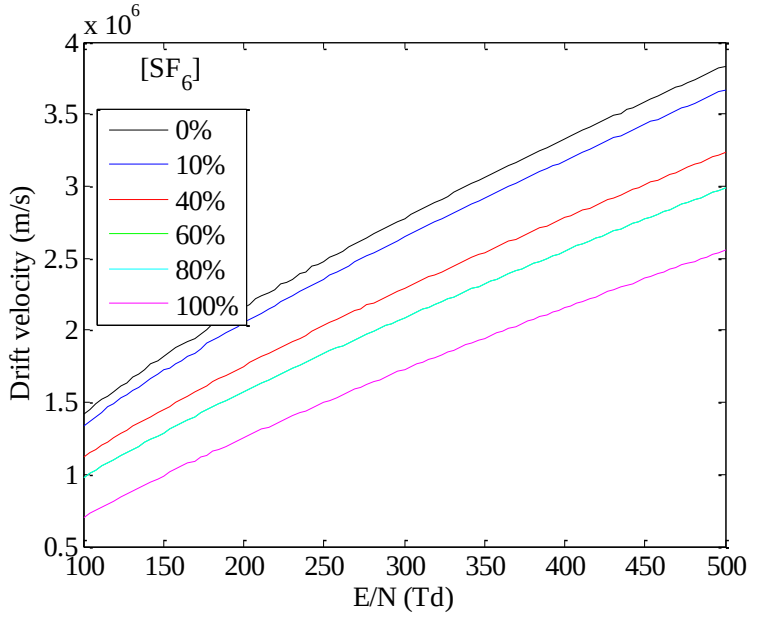

Figure 22: Drift Velocity in SF_6-CO_2 mixtures calculated using Bolsig+

This difference may be attributed to the electron energies at which the electron scattering cross sections for the two additive gases peak. The total electron scattering cross sections for N_2 and CO_2 are shown in Figure 23 and Figure 24. The electron scattering cross-section for N_2 peaks between 2 eV and 3 eV while for CO_2 the electron scattering cross

section has peaks below 0.1 eV, at 4 eV and at 40 eV. The numerous peaks of N_2 at low energies efficiently slow down the electrons at low electric fields while the peaks of the CO_2 at higher energies enable the reduction of electron speed at higher electric fields.

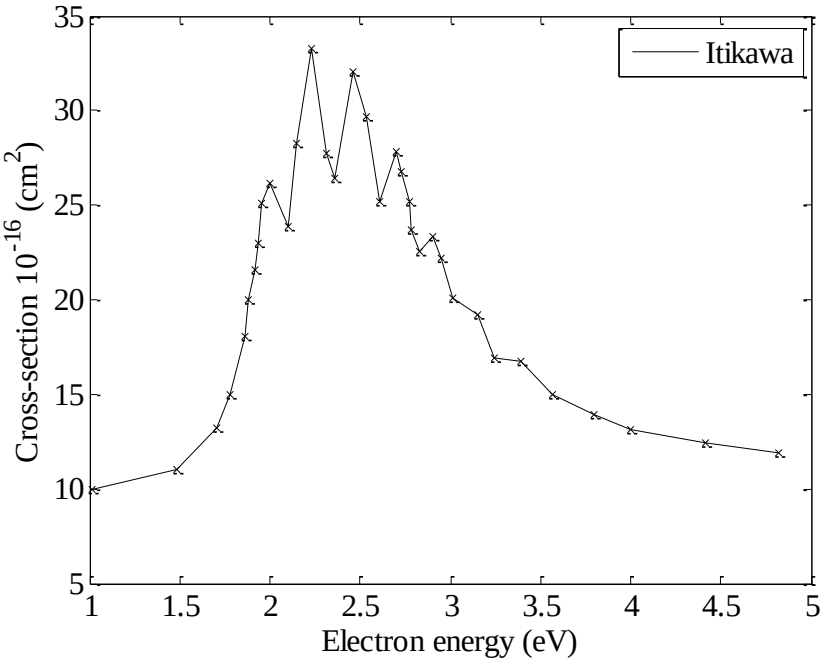

Figure 23: Total electron scattering cross-section of N_2 [55]

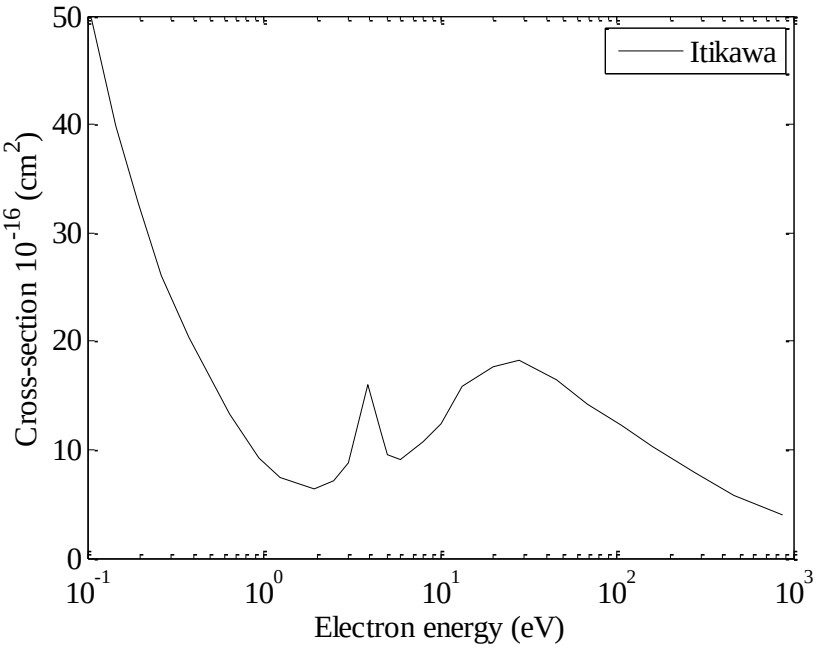

Figure 24: Total electron scattering cross-section for CO_2 [56]

2.5.2 Discussion

The mean energy, EEDF, effective ionisation coefficients, and the electron drift velocity for SF_6-N_2 and SF_6-CO_2 mixtures are calculated using the Boltzmann equation solver Bolsig+ over the number density reduced electric field 100 Td to 500 Td. Comparison of electron coefficients obtained from Bolsig+ and experimental results show good agreement validating the use of Bolsig+ for solving electron coefficients for the fluid model.

As the SF_6 content in the gas mixtures increase, the EEDFs tend to decrease by shifting to lower energies resulting in a reduction of the mean energy of the mixtures. A lower mean energy is representative of fewer high speed/energy electrons, which are necessary for impact ionisation to occur, thus breakdown is less likely.

The SF_6-N_2 mixtures mean energy is lower than the SF_6-CO_2 mixtures with a minimum occurring around 50% SF_6 content. The minimum mean energy occurring at 50% SF_6 content in the SF_6-N_2 mixture suggests that under steady state conditions the synergy between the two gases results in superior performance to pure SF_6 as the optimum ratio of electron slowing down and electron attaching is reached.

The effective ionisation coefficients decrease with increasing SF_6 content and increase with increasing electric field strength. A comparison of the critical electric field strengths of SF_6-N_2 and SF_6-CO_2 show that $(E/N)_{lim}$ is much higher for the SF_6-N_2 mixture than for the SF_6-CO_2 mixture.

The drift velocity increases with increasing electric field and reduces with increasing SF_6 content. At a fixed E/N SF_6-N_2 mixtures tend to possess a lower drift velocity than the SF_6-CO_2 mixtures. With a lower drift velocity electrons are less likely to gain sufficient energy to cause impact ionisation.

Comparison of the SF_6-N_2 and SF_6-CO_2 mixtures demonstrate from a physics point of view (through the mean energy and the effective ionisation and drift velocities) that under steady state conditions the replacement of pure SF_6 by a SF_6-N_2 mixtures is more viable than replacement by a SF_6-CO_2 mixtures.

3 Modelling of Gas Breakdown

Since Townsend described the laws governing ionisation and gaseous discharge in uniform electric fields there has been considerable effort exerted to better understand the development and transition from non-sustained to self-sustained discharge and to accurately determine the breakdown characteristic of a gas [57]. Knowledge of the growth and propagation of charge in a gases and its dielectric characteristic is of critical importance as it leads to better system design [58].

Generically, the application of a sufficiently high electric field results in a conducting channel bridging the gap between the electrodes, through either the avalanche or streamer mechanism, resulting in the collapse of the applied voltage and electrical breakdown.

While the Townsend and Streamer mechanism may be used to determine the breakdown strength of a gas they require a detailed knowledge of the electric fields within the gas during breakdown. These fields are difficult to determine due to the dynamic nature of the space charge formation and its effect on the applied electric field. This is further complicated under impulse conditions when the applied voltage and hence the applied electric field is not steady [18]. As a result, the Townsend and Streamer mechanisms are generally unable to account for the dynamic behaviour of gas discharge.

To account for the dynamic nature of the gas discharge requires a description of the gas at a microscopic level. While the ions undoubtedly play a role in the breakdown of the gas, along with photoemission, the key particle that determines the breakdown of the gas is the electron. Thus to describe the breakdown of a gas at a microscopic level requires the complete description of the dynamic behaviour of the electrons.

There are two kinds of complete descriptions available for the dynamic behaviour of the electrons: the distribution function which obeys the Boltzmann function also known as the fluid model and the individual description which traces the position of each particle such as a Monte Carlo simulation [58] [59] [60]. The individual description of the dynamic behaviour of the electron would be ideal but in practice is impractical due to the large number of particles and the resultant computation time required [58] [61]. Hybrid models exists which reap the advantages of both the fluid and kinetic model [62]. The focus of this work is on the fluid model of gas discharge.

3.1 The Fluid Model of a Gas Discharge

The simplest set of equations containing the basic physics necessary for gaseous discharges are the continuity equations for electrons and ions (to account for the development of the electron and ion densities) coupled with Poisson's equation (to account for the electric field) [60] [61] [63].

Initially developed by Boris and Book [64] to deal with very steep density gradients that appear in shock wave solutions of the transport equations for fluids, Morrow et al applied the flux corrected transport algorithm to the solution of transport of charged particles in a gaseous system [65]. The work proved the basis for the modelling of gas discharges [17]. Due to the solution of 1D drift diffusion equations and the 2D electric field, their work is considered 1.5D.

Further enhancements to the 1.5D FCT-FDM model resulted in improved modelling accuracy with the development of 2D FCT-FDM models by [63]. However, the FDM schemes used in the FCT limited the shape of the grid, limited the geometries expected in discharges and were computationally expensive. This resulted in Georghiou et al proposing improved finite element FCT methods for analysis of 1D, 2D and 3D gaseous discharge [66] [67].

This work makes use of a 1.5D FCT-FDM model developed by Swanson [17] to understand the breakdown of gas mixtures when the dynamic behaviour of gas discharge is accounted for. While a more complex solution could be developed for the purpose of this research the 1.5D FCT-FDM model was sufficient.

3.1.1 Algorithm

Figure 25 illustrates the algorithm implemented by the fluid model. The gas discharge begins with the introduction of an initiating plasma, consisting of electrons, negative and positive ions, with a net charge of zero. Upon this introduction of the "seed" charge a voltage is applied to the electrode (anode for positive and cathode for negative). From the applied voltage the Laplacian electric field is determined [61]. The development of space charge determines the Poissonian electric field and the sum of the two gives the total electric field. Using the total electric field the Townsend and transport coefficients, predetermined through Bolsig+, are read. The electrons, negative and positive ions are then transported through the applications of the continuity equations. The external circuit

current is determined following the transport of the charged species and is included as a voltage drop in the next iteration of the algorithm.

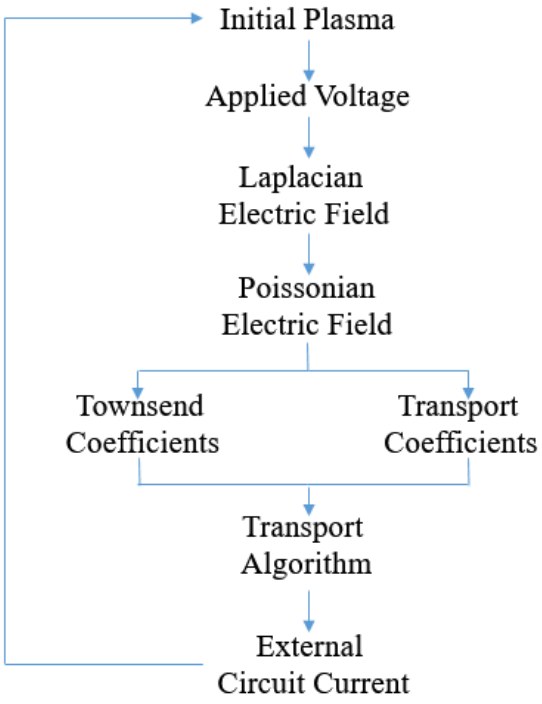

Figure 25: Discharge Algorithm [17]

In order to ensure the absorption of ions and the release of electrons where applicable, boundary conditions are implemented as discussed by Swanson [17].

3.1.2 Continuity Equations

The gaseous discharge is modelled using the continuity equations for electrons, positive ions and negative ions in 1D are given by:

$$\frac{\partial N_e}{\partial t} = N_e\alpha|W_e| - N_e\eta|W_e| - N_eN_p\,\beta - \frac{\partial(N_eW_e)}{\partial z} + \frac{\partial}{\partial z}\left(D_e\frac{\partial^2 N_e}{\partial z^2}\right) \tag{28}$$

$$\frac{\partial N_p}{\partial t} = N_e\alpha|W_e| - N_eN_p\beta - N_nN_p\,\beta - \frac{\partial(\mathrm{N_p}W_p)}{\partial z} + \frac{\partial}{\partial z}\left(D_p\frac{\partial^2 N_p}{\partial z^2}\right)) \tag{29}$$

$$\frac{\partial N_n}{\partial t} = N_e\eta|W_e| - N_nN_p\,\beta - \frac{\partial(\mathrm{N_n}W_n)}{\partial z} + \frac{\partial}{\partial z}\left(D_n\frac{\partial^2 N_n}{\partial z^2}\right)) \tag{30}$$

Where:

$N_{e,p,n} = Number\ densities\ of\ electrons, positive\ ions\ and\ negative\ ions$ (cm^{-3})

$W_{e,p,n} = Velocities\ of\ electrons, positive\ ions\ and\ negative\ ions$ ($\mathrm{cm.\,s}^{-1}$)

$\alpha = Ionisation\ coefficient$ (cm^{-1})

$\eta = Attachment\ coefficient$ (cm^{-1})

$D_{e,p,n} = Diffusion\ coefficients\ of\ electrons, positive\ ions\ and\ negative\ ions$ ($\mathrm{cm}^2.\,\mathrm{s}^{-1}$)

$\beta = Recombination\ coefficient$ ($\mathrm{cm}^3.\,\mathrm{s}^{-1}$)

Note that in order to simplify the model, photo-ionisation has been excluded.

3.1.3 Swarm Parameters

Accurate gas discharge modelling requires an extensive knowledge of the swarm parameters of the gas being modelled [61]. The swarm parameters are used to determine the time dependent densities of charged particles and are needed to solve the continuity

equation for electrons which include the drift, diffusion and multiplication processes [40].

The fluid model can use transport parameters found from the kinetic model or from experimental results where they are obtained through the solution of the stationary Boltzmann equation. The electron transport coefficients used in the model are calculated from the Boltzmann equation solver Bolsig+ (see section 2.5).

The mobility values for positive and negative ions for N_2 and CO_2 are 1.27, 1.84, 0.84 and 0.98 $cm^2 \cdot V^{-1} \cdot s^{-1}$ respectively [25]. The mobility values for the SF_6 positive and negative ions are 0.73 and 1.0 $cm^2 \cdot V^{-1} \cdot s^{-1}$ [68]. In order to simplify the model, the same value of diffusion is used for both the positive and negative ions. As the negative ions tend to have the higher mobilities they are used to calculate the diffusions (see Appendix A). The diffusion values of the ions for N_2, CO_2 and SF_6 used in the model are $0.05, 0.025$ and 0.025 $cm^2 . s^{-1}$ respectively.

3.1.4 Electric Field

The electric field is solved through Poisson's equation:

$$\nabla^2 \phi = -\frac{q_e}{\varepsilon_0}\left(N_p + N_n + N_e\right) \tag{31}$$

Where:

$q_e = Charge\ of\ electron$ (C)

$\varepsilon_0 = Permittivity\ of\ free\ space$ $(F \cdot m^{-1})$

The Laplacian electric field (E_L) is solved through Poisson's equation (using the finite difference method [17]) by setting the number densities to zero.

The space charge (or Poisson) electric field (E_P) is solved using the method of discs as described by Davies [69] where the channel radius r is taken into account and the axial field at a point along the axis is given by:

$$E(x) = \frac{1}{2\varepsilon_0}\int_{-z}^{0} \rho(x+x')\left[-1 - \frac{x'}{\sqrt{x'^2 + r^2}}\right]dx' + \int_{0}^{d-x} \rho(x+x')\left[1 - \frac{x'}{\sqrt{x'^2 + r^2}}\right]dx' \tag{32}$$

The total electric field is then the sum of the Laplacian (applied electric field due to the voltage) and the Poissonian (space charge) electric fields and is given by:

$$E = E_L + E_P \tag{33}$$

3.1.5 Circuit Current

The current I in the external circuit, due to the motion of electrons and ions between the electrodes, is given by Sato's equation modified by Morrow [17]:

$$I(t) = \pi r^2 \frac{q_e}{V_A}\int_0^d \left(N_p v_p - N_n v_n - N_e v_e + \frac{\partial^2 D N_e}{\partial^2 x}\right) E_L dx \tag{34}$$

However, when relating this current to the circuit it will affect the voltage applied to the device under testing. Therefore, the voltage applied to the device under test is given by [17]:

$$V_A = I(t)R - \frac{1}{C}\int I(t)dt \tag{35}$$

Breakdown occurs when the current increases exponentially resulting in the collapse of the voltage. Figure 26 and Figure 27 show the respective withstand and breakdown voltages and currents from the model.

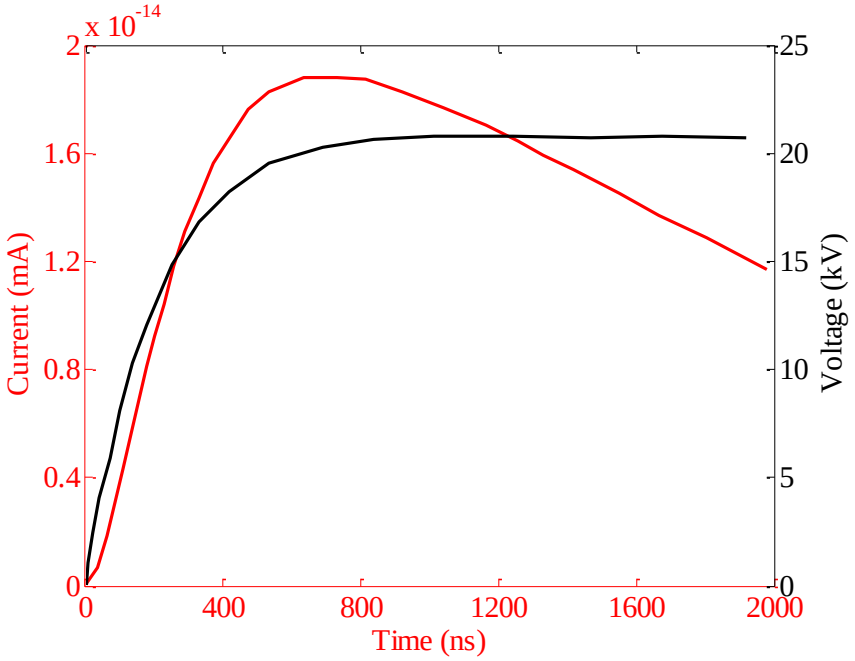

Figure 26: Applied voltage and current during withstand

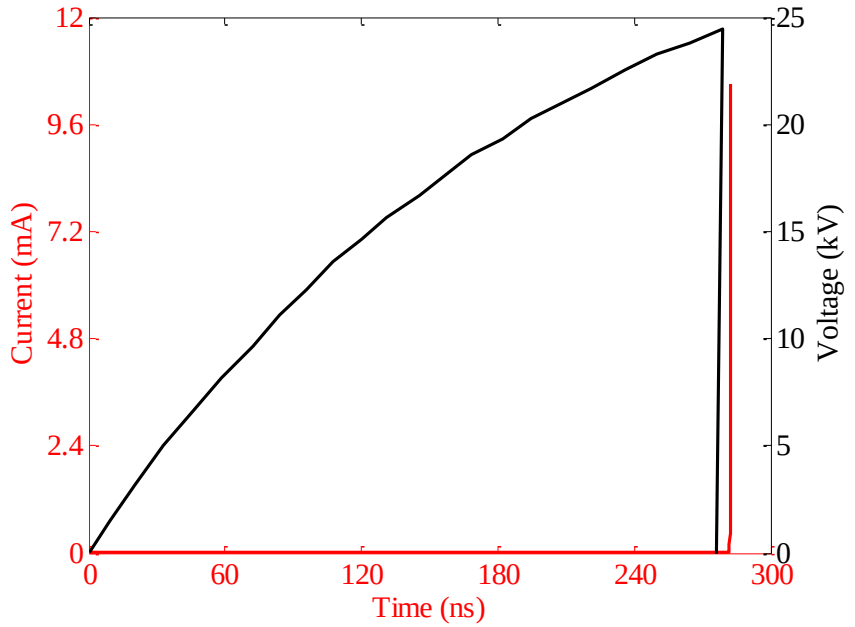

Figure 27: Applied voltage and current during breakdown

3.2 Results

The parameters used in the model for pure SF_6, N_2 and CO_2 are listed in Table 2, where a uniform grid is used. In order for the solution to be meaningful the grid spacing has to be fine close to the electrodes, resulting in a shorter time step [17]. The pressures for the model are the same as the experimental pressures and chosen as discussed in Appendix B. The temperature chosen is the standard room temperature and the electrode spacing is according to the ASTM D2477 standard [70] discussed in section 4. The grid spacing is calculated through the division of the electrode spacing and the grid size as discussed in [17]. The secondary ionisation coefficient used in the model is a weighted sum of the secondary ionisation coefficients of the pure gases obtained from [25].

Table 2: Input parameters for SF_6, N_2 and CO_2

Parameter	Symbol	Value
Pressure	P	100, 200, 300 kPa
Temperature	T	293 K
Electrode spacing	d	2.5 mm
Grid size	Ng	300
Grid spacing	dx	0.009 mm
Time step	dt	20 x 10^{-12}
Secondary ionisation coefficient SF_6, N_2, CO_2	γ	0.26, 0.65, 0.57
Recombination coefficient	β	2 x 10^{-7}
Mobility of positive SF_6 ion	μ_{ps}	0.73 $cm^2 \cdot V^{-1} \cdot s^{-1}$
Mobility of negative SF_6 ion	μ_{ns}	1.0 $cm^2 \cdot V^{-1} \cdot s^{-1}$
Mobility of positive N_2 ion	μ_{pn}	1.27 $cm^2 \cdot V^{-1} \cdot s^{-1}$
Mobility of negative N_2 ion	μ_{nn}	1.84 $cm^2 \cdot V^{-1} \cdot s^{-1}$
Mobility of positive CO_2 ion	μ_{pn}	0.84 $cm^2 \cdot V^{-1} \cdot s^{-1}$
Mobility of negative CO_2 ion	μ_{nn}	0.98 $cm^2 \cdot V^{-1} \cdot s^{-1}$
Diffusion of SF_6 and CO_2 ion	$D_{S,C}$	0.025 $cm^2 \cdot s^{-1}$
Diffusion of N_2 ion	D_N	0.05 $cm^2 \cdot s^{-1}$

An initial plasma number density is applied to the system, giving a peak electron, negative ion and positive ion density at 0.2 mm. The electrons (and ions) are accelerated by the electric field resulting in an initial (although negligible) current. Unless the electric field (sum of the applied and space charge fields) is sufficient to generate new charge carriers breakdown will not occur, as shown in Figure 26.

Should the electric field be sufficiently large, an exponential increase in the number of charge carriers will occur resulting in a spike in the current and the voltage between the electrodes collapsing as show in Figure 27.

A comparison of the breakdown voltage using the model and the U50 lightning breakdown voltage from [71] is illustrated in Figure 28.

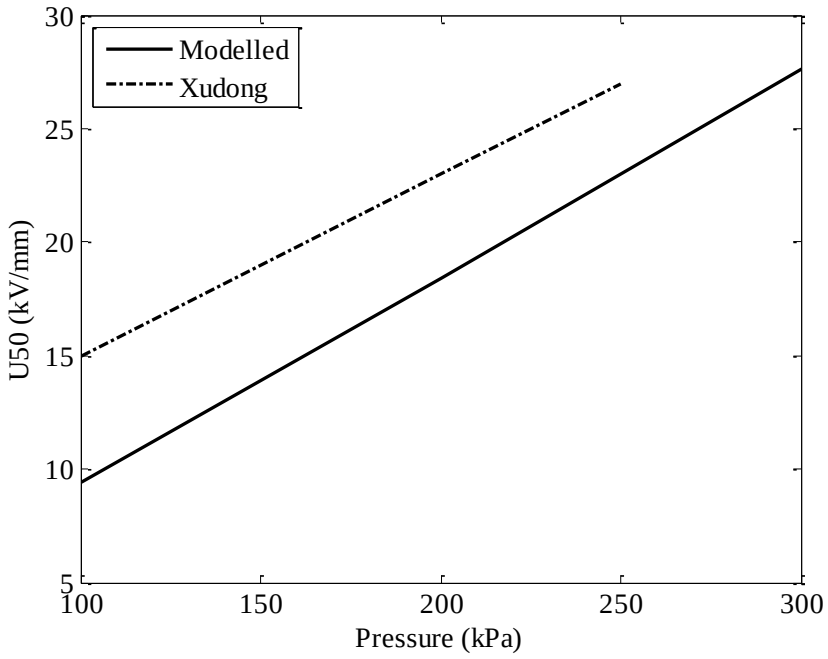

Figure 28: Modelled breakdown voltage of SF_6 under LI for uniform electric field

It can be seen that despite a lower modelled breakdown voltage the trend of the two curves is similar. The difference between the breakdown curves may be attributed to differences between the modelled and experimental electrode configurations as well as due to the modelled breakdown voltage not being the U50 breakdown voltage.

As discussed in section 2.4.2, impulse breakdown is probabilistic in nature. The U50 breakdown voltage is the voltage at which there is a 50% probability of breakdown occurring [25]. However, in the model the probability has been removed as charge is "artificially" inserted into the model.

Thus, breakdown in the model is dependent on the position and magnitude of the "seed" plasma and as long as this remains unchanged the breakdown for a particular gas mixture will be constant.

Differences may also be attributed to the nature of the fluid model which assumes the plasma species are in equilibrium with the electric field, so that the energy gained is normally balanced by the energy lost during collisions (i.e. the continuity equations). This assumption is not always true as gases frequently experience non-equilibrium behaviour [72].

In addition, while the model's inputs from Bolsig+ take into account varying pressures and electric fields for various electron coefficients; the secondary coefficient, recombination coefficient and ion mobilities for the gas remain constant despite changing pressures and electric fields.

3.2.1 SF_6-N_2 Mixtures

The parameters used in the model for SF_6-N_2 mixtures are listed in Table 2. Note that a weighted average of the ion mobilities is used for the mixtures.

Figure 29 shows the modelled breakdown voltage of SF_6-N_2 gas mixtures at pressures of 100, 200 and 300 kPa under the influence positive and negative LI. An increase in the breakdown voltage is observed for increasing SF_6 content and increasing pressure. The greatest increase in breakdown voltage occurs as the SF_6 content is increased from 0% to 30%. This is in good agreement with the mean energies calculated using Bolsig+ (Figure 11). After 30% SF_6 content the increase in breakdown strength is more gradual. There is very little difference between breakdown under positive and negative LI; except for the 100 kPa curve where the positive breakdown voltage is lower until 40% SF_6 content.

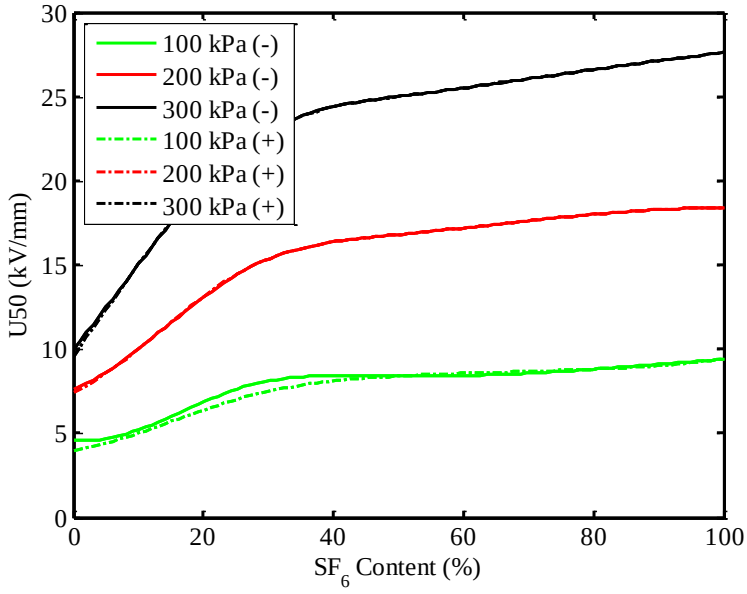

Figure 29: Modelled breakdown voltage of SF_6-N_2 under LI

3.2.1.1 Synergistic effect of SF_6 mixtures

The weighted breakdown values for SF_6 mixtures are based on the breakdown values of the pure component gases. The equation used to calculate the weighted breakdown values for a binary SF_6 mixture is given by:

$$U_W = U_{SF_6} \cdot pS + U_{mix} \cdot (1 - pS) \tag{36}$$

Where:

$U_W = weighted\ breakdown\ voltage$ (kV/mm)

$U_{SF_6} = weighted\ breakdown\ voltage$ (kV/mm)

$U_{mix} = breakdown\ voltage\ of\ pure\ N_2/CO_2$ (kV/mm)

$pS = percentage\ of\ SF_6 in\ the\ mixture$ (%)

In order to demonstrate the synergy effect in the SF_6-N_2 mixture, the modelled and weighted breakdown values are compared in Figure 30. A clear synergistic effect is observed in the mixtures with an increase in pressure increasing the synergy and maximum synergy effect occurring around 30% SF_6 content.

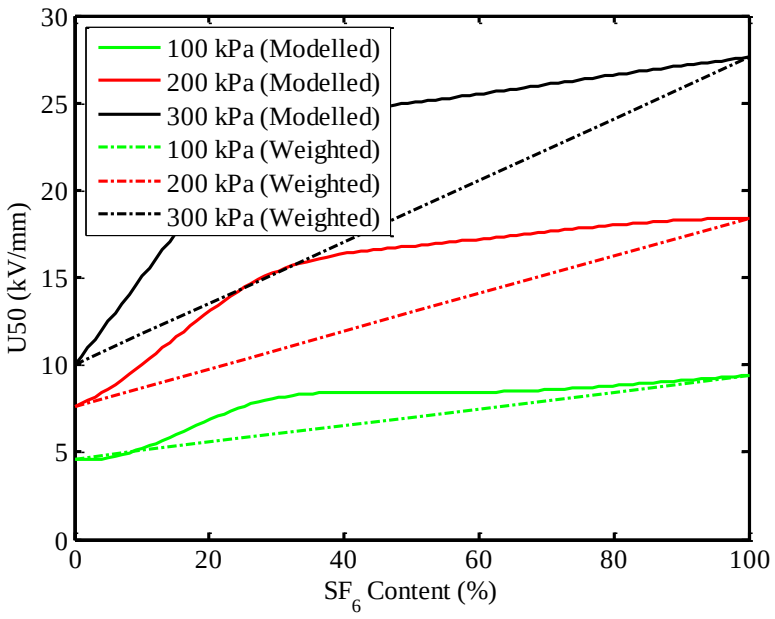

Figure 30: Modelled and weighted breakdown voltage of SF_6-N_2 under LI

3.2.2 SF_6-CO_2 Mixtures

The parameters used in the model for SF_6-CO_2 mixtures are listed in Table 2. As with the SF_6-N_2 mixture a weighted average of the ion mobilities is used for varying SF_6 content within the mixture.

The modelled breakdown voltages of the SF_6-CO_2 gas mixtures for a uniform electric field at pressures of 100, 200 and 300 kPa under positive and negative LI are illustrated in Figure 31 while Figure 32 compares the modelled and weighted breakdown voltages to determine synergy.

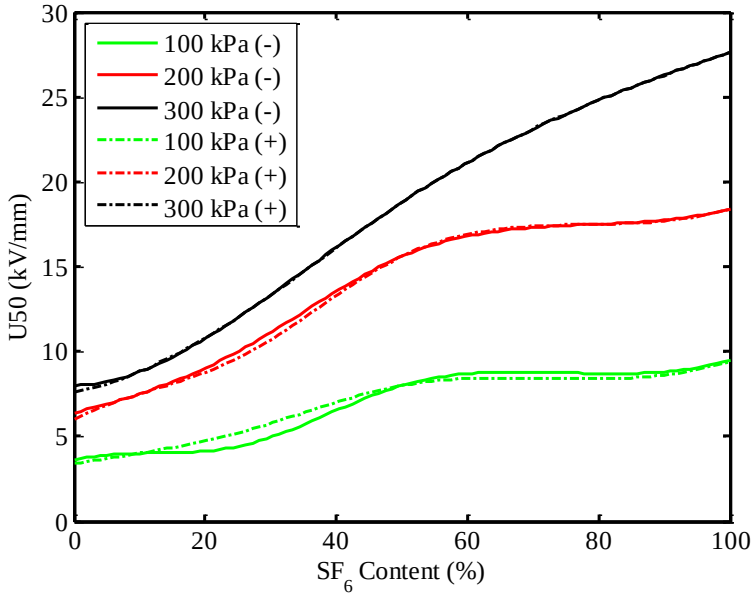

Figure 31: Modelled breakdown voltage of SF_6-CO_2 under LI

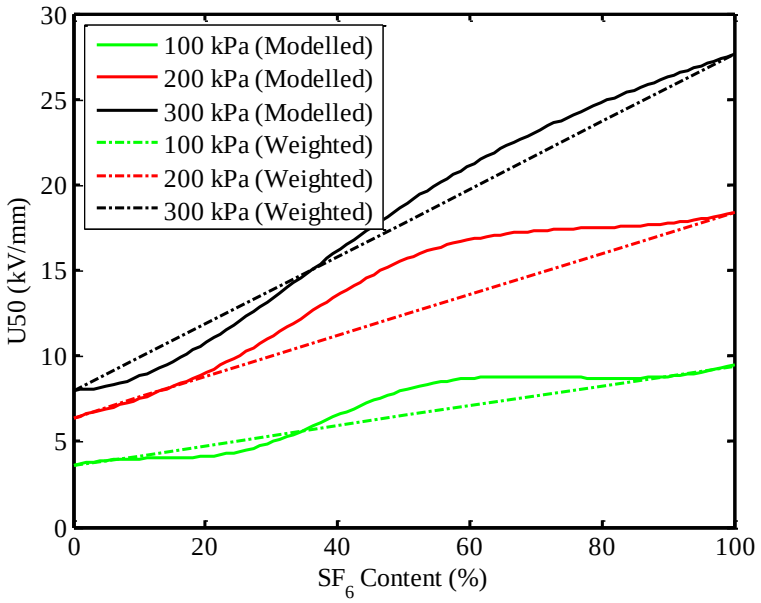

Figure 32: Modelled and weighted breakdown voltage of SF_6-CO_2 under LI

Figure 31 illustrates increasing breakdown voltage with increasing SF_6 content with the greatest increase occurring as SF_6 content is increased from 20% to 50%. The positive and negative breakdown values are similar.

In Figure 32 for SF_6 content greater than 40% a positive synergy effect is observed for all pressures with a maximum synergy occurring around 55% SF_6 content. A negative synergy effect is observed at 100 and 300 kPa where the modelled values lie below the weighted values.

3.3 Discussion

The modelling of the positive and negative breakdown of the SF_6-N_2 mixtures under uniform electric field conditions and LI demonstrate that when the dynamic behaviour of breakdown (the development of space charge) is accounted for, binary mixtures of SF_6-N_2/CO_2 experience a positive synergistic effect. The degree to which synergy is experienced is dependent on the SF_6 content and the pressure of the mixtures.

As observed in Figure 30 the maximum synergy effect for the SF_6-N_2 mixture appears to be around 30% SF_6 content, with increasing pressure improving synergy. The polarity of the applied voltage only has a slight effect on the modelled breakdown values.

Figure 32 illustrates the synergy effect of the SF_6-CO_2 mixtures. It can be observed that the SF_6-CO_2 mixtures exhibit a negative synergy effect at low SF_6 content. A positive synergy effect is only observed for SF6 content greater than 40% with a maximum positive synergy occurring around 50% SF_6 for 100 and 200 kPa and 60% SF_6 content for 300 kPa.

In comparison to the SF_6-N_2 mixture the SF_6-CO_2 mixture experiences negative synergy, experiences positive synergy at much higher SF_6 content and unlike the SF_6 -N2 mixtures whose degree of synergy increases with pressure; experiences a peak synergy at 200 kPa

These differences between the behaviour of the SF_6-N_2 and SF_6-CO_2 mixtures imply that when the dynamic behaviour of gas discharge is accounted for, SF_6-N_2 is a superior replacement to SF_6-CO_2. Not only is the performance of the SF_6-N_2 mixture more consistent but the synergy effect is stronger and peaks at a much lower SF_6 content making it more environmentally acceptable.

The conclusions extracted from this model requiring experimental validation are:

- The influence of increasing the pressure of a mixture on the degree of synergy.
- The SF_6 content at which maximum synergy is observed.
- The superiority of SF_6-N_2 over SF_6-CO_2.

4 Experiment Details

Testing involved the measurement of the LI breakdown voltages of SF_6-N_2/CO_2 mixtures as SF_6 content (0% to 100%) and pressure (100 kPa to 300 kPa) were varied under a uniform electric field. The experiment was conducted using the ASTM D2477 standard [70] for the preparation of the pressure vessel and the Up-Down Method [73] for the recording and calculation of the breakdown voltage.

4.1 Experimental Apparatus

LI voltages (1.2/50 μs), of up to 90 kV were generated by a Marx generator. The measurement system consisted of a capacitive divider, shielded coaxial cable, resistance matching circuit, RIGOL DS1052E oscilloscope and HAEFFLY impulse voltmeter, illustrated in Figure 33.

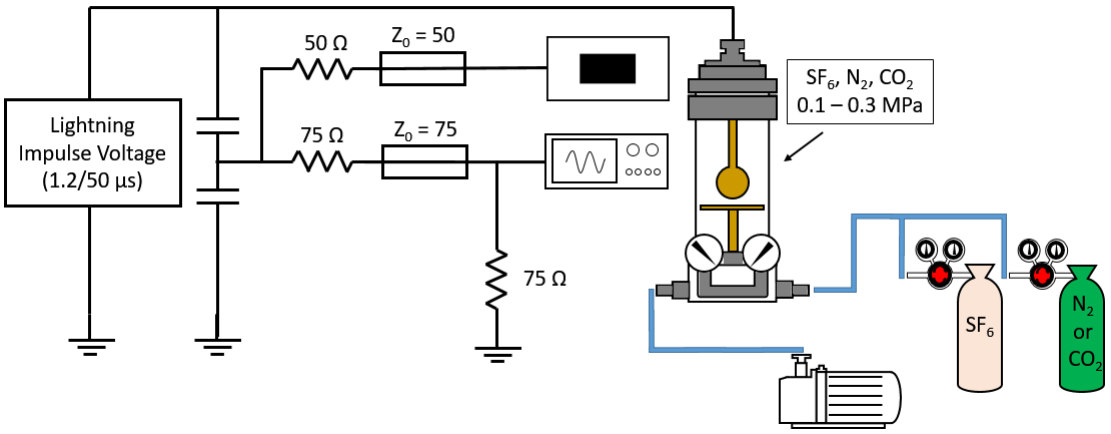

Figure 33: Testing arrangement

The pressure chamber used was built by Messwandler-Bau GMBH in 1982. The chamber is cylindrical with a diameter of 132 mm, a total internal volume of 6 dm^3, a maximum operating temperature of 35 ^oC, a maximum test pressure of 650 kPa and two inlet/outlet valves. The Perspex walls of the chamber caused no distortion to the field of the electrodes.

Following the ASTM D2477 standard a sphere-plane electrode gap was set up in order to obtain a uniform field [70]. The electrode configuration, dimensions, materials and electric field (calculated using FEMM) are shown in Figure 34.

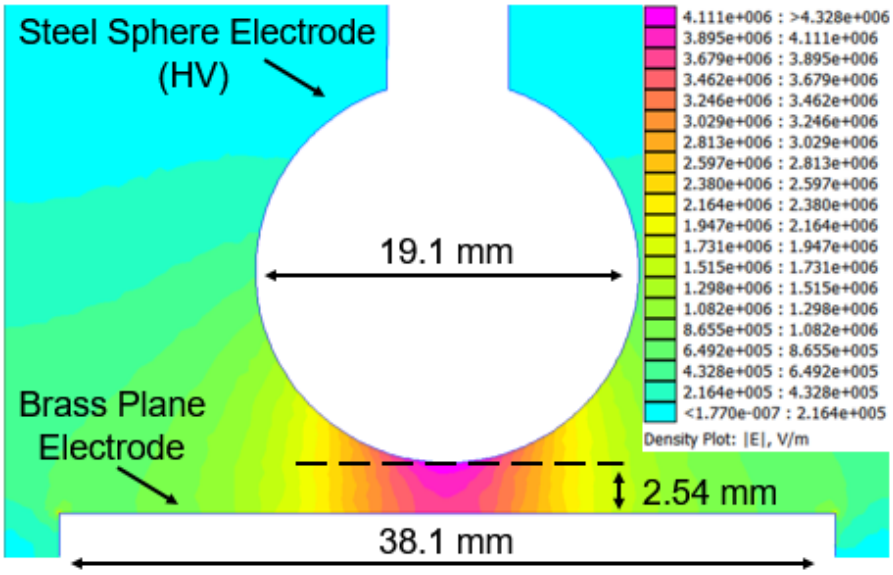

Figure 34: Arrangement of electrodes used

The gases were obtained from Afrox in 31.1 kg, 11.0 kg and 9.0 kg canisters for CO_2, N_2 and SF_6 respectively. The gases were of 99.0% purity. Afrox multistage scientific regulators were used to dispense the gas. Standard 8 mm hose was used to connect the regulators to the pressure chamber.

4.2 Experimental Method

Before the placement of the gas inside the test chamber the vessel was prepared according to the ASTM D2477 standard [70]. Using Dalton's law of partial pressures, the individual gases were placed inside the pressure chamber and left to mix for a minimum of 2 hours in order to ensure a uniform mixture [8]. The SF_6 was always placed into the vessel first.

The 50% breakdown voltages under LI were determined using the Up and Down method with a minimum of 20 breakdown values being recorded [73]. The time interval between successive shots was 3 minutes to allow for the recovery of the dielectric strength of the gas.

Before recording any values the system was "spark conditioned" as described by Cookson [32]. Conditioning is defined as "the increase in the breakdown voltage by the test procedure" [32] and is the increase in the breakdown voltage as the number of breakdowns increases until a plateau is reached. The amount of spark conditioning required is dependent on the electrode area and electrode surface condition [18] [32]. A

minimum of 20 breakdowns occurred to ensure conditioning, however, the plateau was usually reached in 5-10 breakdowns.

4.3 Results

4.3.1 Breakdown Characteristics of SF_6-N_2

4.3.1.1 Measured breakdown values of SF_6-N_2 mixtures

Figure 35 shows the measured breakdown voltage of SF_6-N_2 gas mixtures at pressures of 100, 200 and 300 kPa under uniform electric field and positive and negative LI as the SF_6 content was varied. While the trend of the curves shows that an increase in SF_6 content and an increase in pressure will result in a higher LI breakdown voltage; there is a marked difference between the behaviour of the positive and negative LI.

For the positive LI it can be seen that as SF_6 content is increased from 0% to 40% there is a gentle increase in the breakdown voltage for all pressures. Further increase of the SF_6 content resulted in a steeper rise of the breakdown voltage.

The negative LI curves exhibit a sharp rise in the breakdown voltage as SF_6 content is increased from 0% to 25 %. Thereafter, an increase in SF_6 content results in a decrease in the breakdown voltage with the minimum occurring around 50% SF_6 content. A further increase in SF_6 content increases in the breakdown voltage. An increase in pressure results in a more pronounced local maximum.

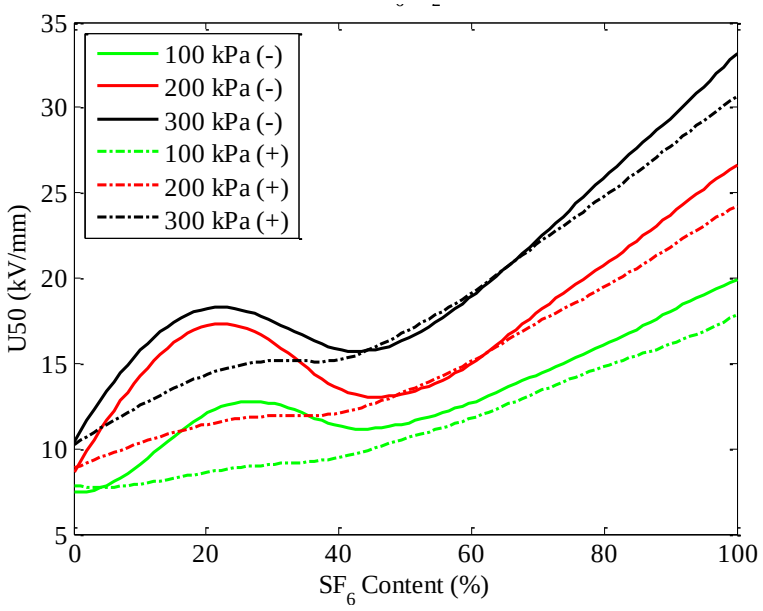

Figure 35: Measured breakdown voltage for SF_6-N_2 under LI

4.3.1.2 Synergistic effects of SF_6-N_2 mixtures

In order to clearly illustrate the synergy effect, the measured and weighted breakdown voltages for SF_6-N_2 mixtures under negative and positive LI are compared in Figure 36 and Figure 37.

For a negative LI a positive synergy effect (whereby the measured breakdown voltage is higher than the weighted breakdown) is observed around 20% to 25% SF_6 content as shown in Figure 36. An increasing pressure results in the local maximum breakdown voltage shifting from 25% to 20% SF_6 content. As the SF_6 content is increased past 30% a negative synergy effect occurs.

Under positive LI a slight positive synergy is observed for the 200 and 300 kPa curves with SF_6 content below 20% and 25% respectively. As the SF_6 content is increased a negative synergy occurs. The 100 kPa curve experiences negative synergy irrespective of SF_6 content.

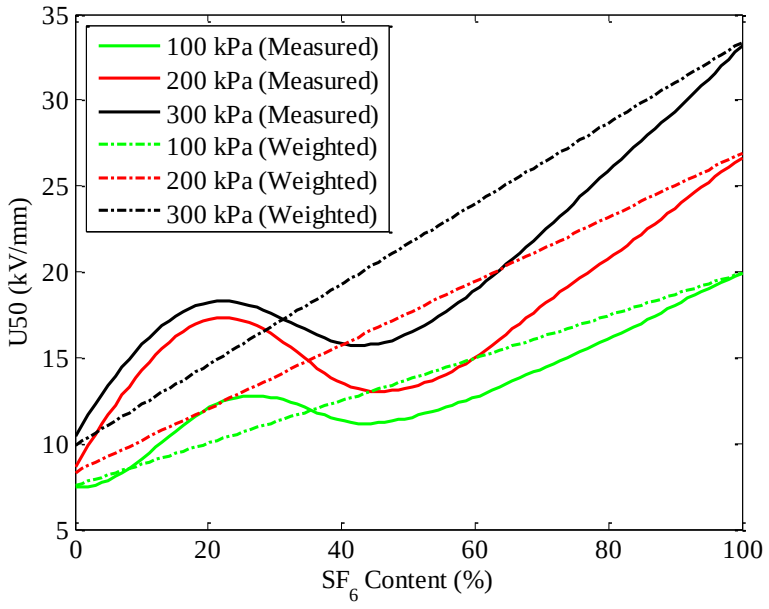

Figure 36: Measured and weighted breakdown voltage of SF_6-N_2 under negative LI

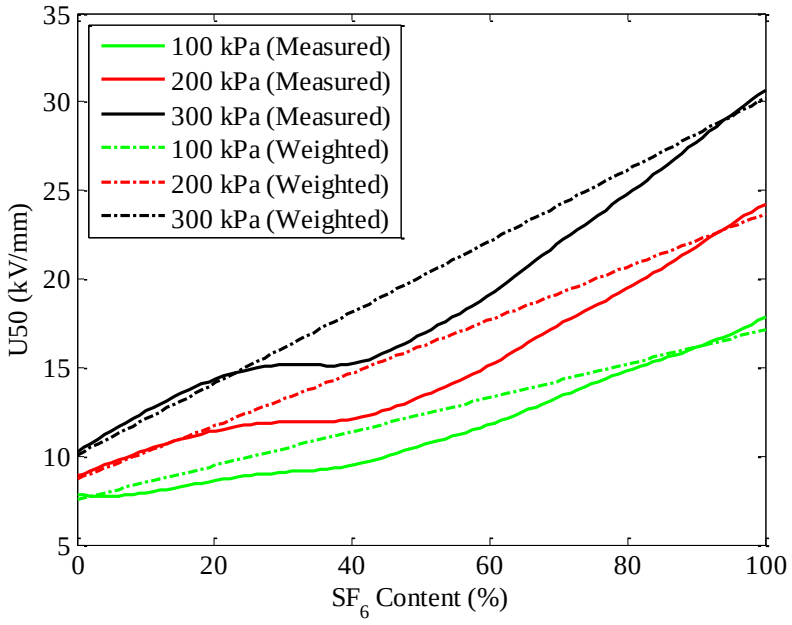

Figure 37: Measured and weighted breakdown voltage of SF_6-N_2 under positive LI

4.3.1 Breakdown Characteristics of SF_6-CO_2

4.3.1.1 Measured breakdown values of SF_6-CO_2 mixtures

The breakdown voltage of the SF_6-CO_2 gas mixtures for a uniform electric field, at pressures of 100, 200 and 300 kPa and under positive and negative LI are shown in Figure 38. It can be seen that the breakdown voltage tends to increase with increasing SF_6 content and with increasing pressure. It is apparent that, as with the SF_6-N_2 mixture, the breakdown behaviour under positive and negative LI is quite different.

At 200 and 300 kPa the negative LI breakdown voltage curves have three distinct gradients. From 0% to 25% SF_6 content there is a gentle increase in breakdown voltage. From 25% to 50% there is a steeper rise in the breakdown voltage and thereafter, an increase in the breakdown voltage results in a gentle rise in the breakdown voltage. For the 100 kPa negative impulse breakdown curve there is a gentle increase in the breakdown voltage until 40% SF_6 content from which there is a rapid increase in the breakdown voltage as SF_6 content is increased.

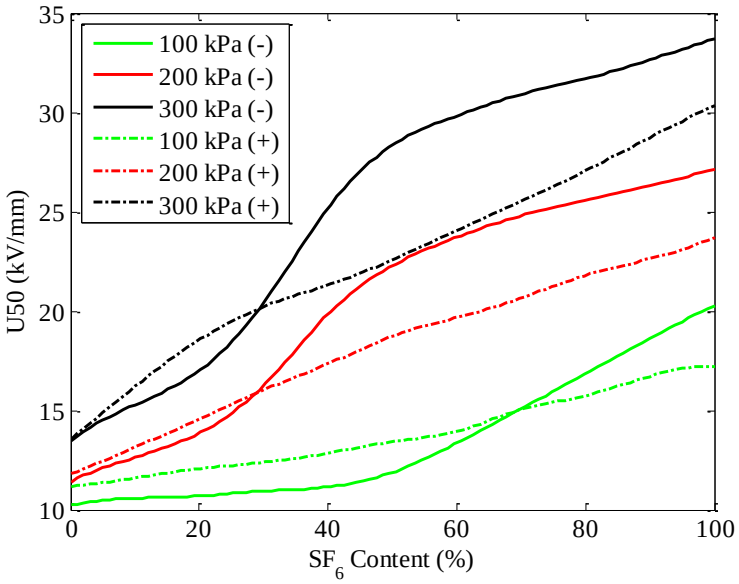

Figure 38: Measured breakdown voltages for SF_6-CO_2 under LI

The positive LI curves for SF_6-CO_2 mixtures appear to exhibit similar behaviour showing increasing breakdown strength with increasing SF_6 content. The gradient of the positive LI curves tend to increase with pressure.

4.3.1.1 Synergistic effects of SF_6-CO_2 mixtures

Figure 39 and Figure 40 show the synergistic effects of SF_6-CO_2 mixtures under positive and negative LI. It is clear that the polarity of the applied voltage and the pressure play an important role in synergistic effects in SF_6-CO_2 gas mixtures. The 100 kPa curves of both polarity of LI display negative synergy effect. The 200 and 300 kPa negative LI curves show negative synergy below 30% SF_6 content and positive synergy above it, with a peak positive synergy occurring around 50% SF_6 content.

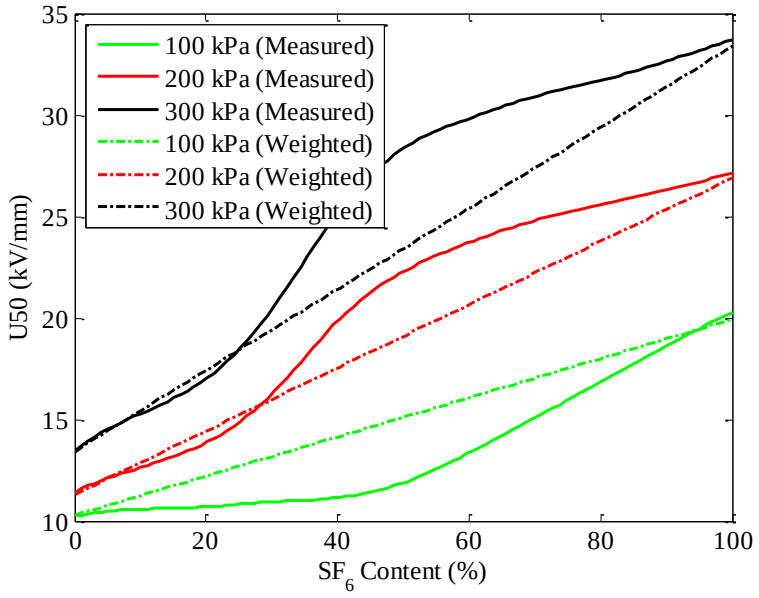

Figure 39: Measured and weighted breakdown voltage of SF_6-CO_2 under negative LI

For the positive LI at 200 and 300 kPa there is only positive synergy with a peak around 25% SF_6 content for 300 kPa and 50% SF_6 content for 200 kPa.

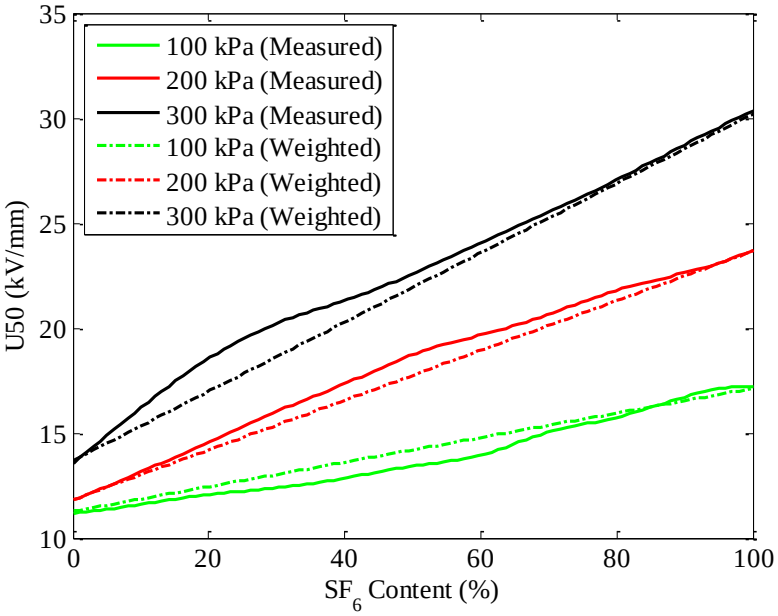

Figure 40: Measured and weighted breakdown voltage of SF_6-CO_2 under positive LI

4.4 Discussion

The LI breakdown voltage of binary SF_6-N_2/CO_2 mixtures are obtained, under uniform electric field conditions, for positive and negative polarity, as SF_6 content in the mixture and the pressure of the mixture are varied. Comparison of the experimentally obtained

breakdown values with the weighted breakdown values illustrate the synergistic effects that occur in these binary mixtures.

Both SF_6-N_2 and SF_6-CO_2 gas mixtures show that their breakdown voltage behaviour is dependent on the polarity of the applied impulse, the pressure of the gas mixture and the SF_6 content of the mixture. Breakdown under negative LI tends to be higher than under positive LI. SF_6-CO_2 mixtures tend to have a higher breakdown voltage than SF_6-N_2 mixtures especially at higher SF_6 content.

SF_6-N_2 mixtures show positive and negative synergistic effects under both polarities of LI. Under negative LI strong positive synergy occurs for SF_6 content below <25% followed by a strong negative synergy as SF_6 content is increased. Under positive LI a weak positive synergy is observed for SF_6 content below 20% with a strong negative synergy for increased SF_6 content. Positive LI at 100 kPa always displays negative synergy.

SF_6-CO_2 mixtures show positive and negative synergistic effects under both polarities of LI. Under negative LI a weak negative synergy effect occurs for low SF_6 content with an increase in SF_6 resulting in a strong positive synergy. Under positive LI a weak positive synergy is observed for all SF_6 content.

Under uniform electric field conditions at pressures greater than 100 kPa, SF_6-N_2 is a viable replacement for pure SF_6 at SF_6 content below 25%. SF_6-CO_2 is a viable replacement at SF_6 content greater than 30%. SF_6 content greater than or less than these respective values and at lower pressures results in undesirable negative synergy.

The experimental results suggest that SF_6-CO_2 would be better suited to the replacement of pure SF_6 than SF_6-N_2 as it tends to have a much higher breakdown voltage even when experiencing negative synergy.

5 Comparison of Modelled and Experimental Results

5.1 SF_6-N_2 Mixtures

Figure 41 illustrates the modelled and experimental breakdown voltages for the SF_6-N_2 mixtures under negative LI and uniform electric field conditions as pressure and SF_6 content is varied. For the 100 kPa, 200 kPa and 300 kPa curves it can be observed that there is a similar trend between the modelled and experimental results for SF_6 content below 25%. Above 25% SF_6 content the modelled and experimental results diverge and the experimental results demonstrate a negative synergy.

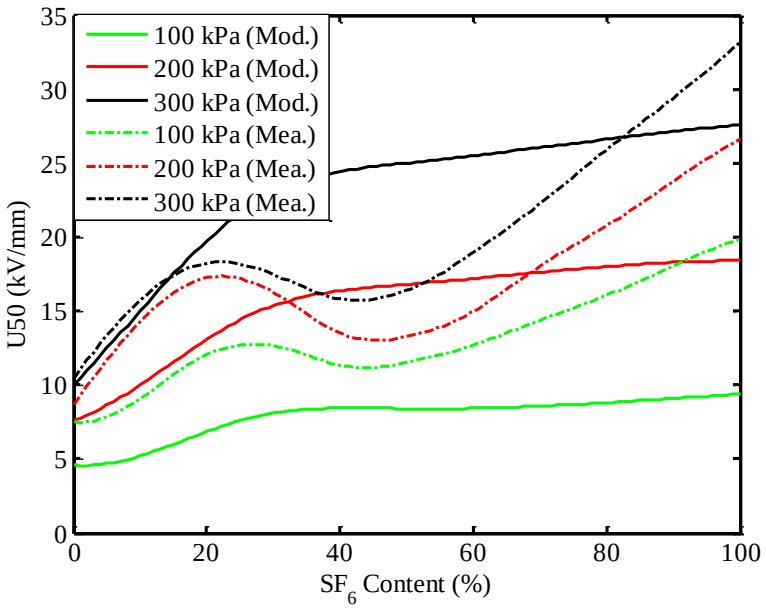

Figure 41: Modelled and measured breakdown of SF_6-N_2 under negative LI

Figure 42 compares the modelled and experimental breakdown voltages of the SF_6-N_2 mixtures under positive LI and uniform electric field conditions as pressure and SF_6 content is varied. For the 200 kPa and 300 kPa curves increasing SF_6 content results increasing breakdown voltage until 30% SF_6 content for the modelled and experimental results after which the experimental results experience negative synergy. The modelled and experimental curves at 100 kPa demonstrate no appreciable similarities.

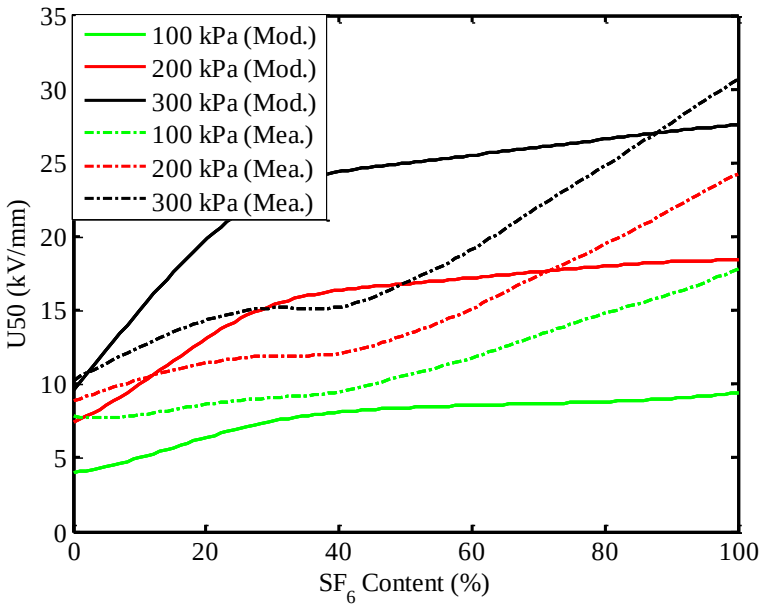

Figure 42: Modelled and measured breakdown of SF_6-N_2 under positive LI

5.2 SF_6-CO_2 Mixtures

Figure 43 illustrates the correlation between the modelled and experimental results for SF_6-CO_2 mixtures under negative LI. It can be observed that the breakdown voltages do not coincide for the modelled and experimental results for the pure gases or for the mixes. However, it can be seen that both the modelled and breakdown curves for 200 kPa and 300 kPa have a similar shape. The 100 kPa experimental curve is dissimilar to the other experimental curves and dissimilar to the modelled results.

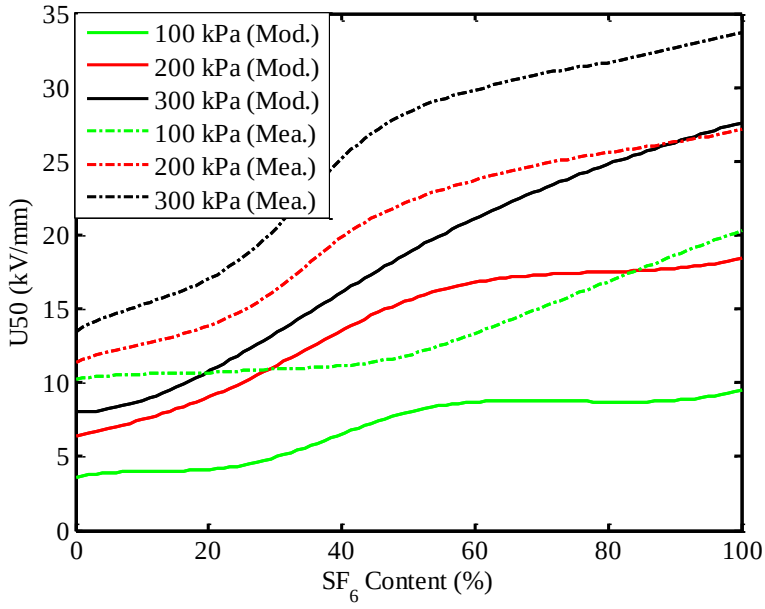

Figure 43: Modelled and measured breakdown of SF_6-CO_2 under negative LI

Figure 44 illustrates the breakdown voltage of the SF_6-CO_2 mixtures under positive impulse. There appears to be very little correlation between the modelled and measured impulse except for the trend of both showing increasing breakdown voltage as SF_6 content is increased.

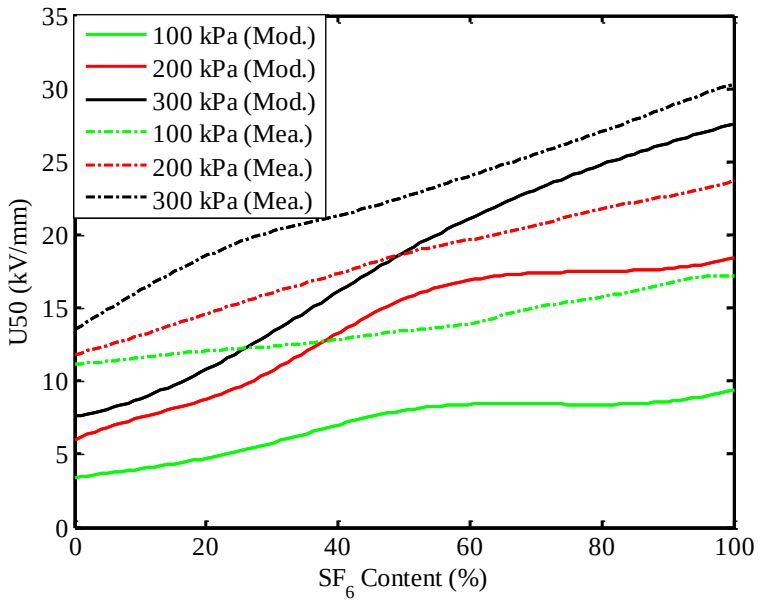

Figure 44: Modelled and measured breakdown of SF_6-CO_2 under positive LI

5.3 Discussion

A comparison of the modelled and experimentally obtained values for the breakdown voltage of SF_6-N_2/CO_2 mixtures as SF_6 content, pressure and polarity of LI are varied illustrate significant differences between the modelled and experimental results especially in SF_6-N_2 and for positive SF_6-CO_2. These differences may be accounted for by the intrinsic characteristics of the fluid model, the inputs into the fluid model and electrode effects.

Intrinsic characteristics of the fluid model itself will result in a difference between the modelled and experimental results. The fluid model is an approximation that assumes the electrons are in equilibrium with the electric field. This is not always true as electrons in strong electric field regions may gain more energy from the field than they lose during collisions, thereby, resulting in non-equilibrium behaviour [72]. Secondly the model is not 3D. The model is not even 2D. The transport equations responsible for the movement of the charged particles are solved in 1D and the electric field is solved in 2D. In addition, photo-ionisation was excluded from the model. It follows that due to its simplicity (using

fewer dimensions and excluding effects such as photo-ionisation) the modelled results would differ from the experimental results. However, these intrinsic shortcomings were only expected to affect the magnitude of the breakdown voltages obtained from the model with similar trends still being observed as SF_6 content was increased.

Inputs for the model strongly affect the accuracy of the model. The ion mobilities were weighted averages of the two pure gases and not related to the actual number density of the ions in the gas. Despite their being a number of species of negative/positive ions in the SF_6-N_2/CO_2 mixtures, they were treated as one (a single species of positive ions and a single species of negative ions). The recombination coefficient remained unchanged by gas composition and number density. The secondary ionisation coefficient remained unchanged by differing gas composition.

Another possible reason for the discrepancy between the modelled and experimental results lie in the electrodes and their effect on the electric field, specifically the effect of surface roughness on the electric field [74]. The model assumes a uniform electric field with no surface defects, however, the experiment uses a uniform field with electrodes that may contain defects. These electrode defects will result in non-uniformity in the electric field. Field uniformity has a strong impact on the breakdown in mixtures containing SF_6 as shown in Figure 45 and Figure 46 where breakdown for pure SF_6 mixtures is shown for uniform and non-uniform electric fields.

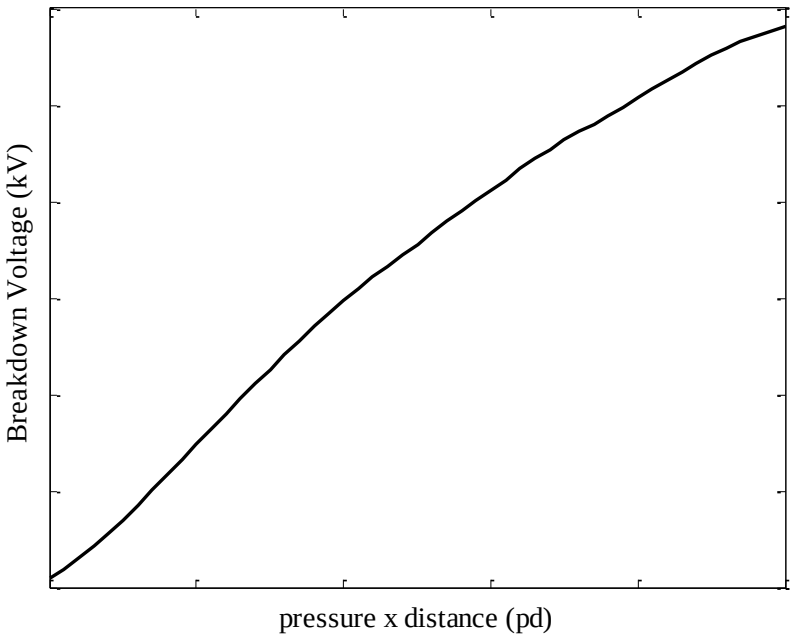

Figure 45: Breakdown under a uniform electric field in SF_6 [75]

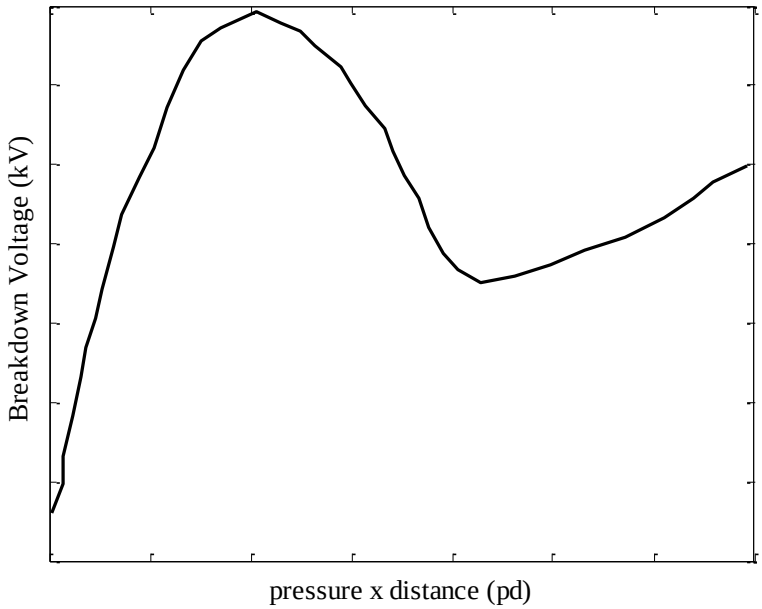

Figure 46: Breakdown under a non-uniform electric field in SF_6 [75]

Despite the obvious difference between the modelled and experimental results the model does indicate that positive synergy will occur for both SF_6-N_2 and SF_6-CO_2 mixtures when the dynamic behaviour of gas discharge is taken into account.

In addition, the greatest increase in the modelled breakdown voltage for the SF_6-N_2 mixture under negative and positive LI occurred from 0% to around 25% SF_6 content which is the same SF_6 content at which positive synergy is experienced for the experimental results. The SF_6-CO_2 modelled breakdown voltages under negative LI show similar trends to the experimental results, however, under positive LI differed greatly.

6 Conclusions and Recommendations

The breakdown strength of an SF_6-buffer gas mixture is strongly influenced by the ability of the buffer gas to reduce free electron energies sufficiently to allow the SF_6 molecules to remover them. This process of energy/speed reduction occurs through scattering and occurs with a time constant characteristic of the fundamental processes in gas discharge. As a result, a difference of efficiency of synergy is expected between steady state and LI which occurs with a rise time on the same order of magnitude as the fundamental processes.

In this work the synergy effect (and hence the suitability) of SF_6-N_2 and SF_6-CO_2 mixtures under LI was investigated through a model that accounted for the dynamic processes of gas discharge (the formation of space charge) and through experimentation. Under uniform electric fields the SF_6 content was varied for pressures of 100, 200 and 300 kPa.

The steady state solution of the Boltzmann equation, the 1.5D FCT-FDM model and experimentation indicated synergy in both mixtures. However, there were noticeable differences between the modelled and measured results.

From the theory and modelling, the SF_6-N_2 mixtures appear to possess superior performance characteristics to the SF_6-CO_2 mixtures as they demonstrate a lower mean energy, higher critical field strength, stronger synergy effect and show significant improvement in their dielectric strength at low SF_6 content (<25%). In addition, the SF_6-N_2 mixtures displayed only positive synergy when modelled, whereas the SF_6-CO_2 mixtures displayed negative synergy for SF_6 content below 30%. The theory and model also suggested slight to negligible differences between positive and negative LI.

Contrary to both the theory and the model; the experimentation indicated that the polarity of the LI plays an important role in the breakdown strength and synergy of a gas with it playing a greater role as SF_6 content is increased. At higher levels of SF_6 content both SF_6-N_2 and SF_6-CO_2 mixtures exhibited higher breakdown voltages under negative polarity. The experimentation indicated that SF_6-CO_2 mixtures would be a better replacement for pure SF_6 as it possesses a higher breakdown strength than the SF_6-N_2 mixtures. In addition, the SF_6-CO_2 mixtures only experienced negative synergy under negative LI whereas the SF_6-N_2 mixtures experienced negative synergy under both polarities of LI.

6.1 Recommendations

The following recommendations are made:

- Include photo-ionisation within the model as it is believed that this would decrease the modelled breakdown voltage of SF_6 [68].
- Use separate ion mobilities for the individual gases in the mixture. For example, in the SF_6-N_2 mixture there needs to be a positive ion mobility for the SF_6 ions and a separate positive ion mobility for the N_2 ions. The same needs to occur for the negative ions.
- Use a recombination coefficient that is dependent on pressure/number density and nature of gas and ensure the secondary ionisation coefficient changes according to gas composition.
- The boundary conditions were difficult to predict so require greater attention.
- Implement a full three-dimensional model to reduce approximations within the fluid model.
- Investigate the effect of surface roughness on the breakdown of SF_6 mixtures as it is believed to be partly responsible for the negative synergy effect observed during experimentation.

7 References

[1] T. Govender, “Identifying Defects in SF6:N2 Mixtures using External UHF Couplers and Neural Network Analysis,” University of the Witwatersrand, Johannesburg, 2011.

[2] D. Jeong, S. Woo, K. Seo and J. Kim, “A Study of the Insulation Property for Development of Eco-friendly GIS Under SF6/N2 Mixtures,” in *1st International Conference on Electric Power Equipment*, Xi'an, 2011.

[3] M. Koch, “Prediction of Breakdown Voltages in Novel Gases for High Voltage Insulation,” PhD Dissertation, Aachen University, Zurich, 2015.

[4] Naveen, R. Verma and S. Dahiya, “CDM inSub-Stations by Replacement of SF6 Gas in Circuit Breaker,” *International Journal of Innovations in Engineering and Technology*, vol. 1, no. 4, pp. 8-16, 2012.

[5] H. Zhao, X. Li, A. Murphy and S. Jia, “Investigation of Dielectric Breakdown Properties of SF6-N2 and SF6-CF4 Mixtures at 0.4MPa and Gas Temperatures up to 3000K”.

[6] A. Lemzadmi, F. Beloucif, A. Guerroui and A. Denat, “Iception Corona Discharge Voltages in SF6-N2 Gas Mixtures at High Gas Pressure,” *International Journal on Electrical Engineering and Informatics*, vol. 6, no. 1, pp. 195-202, 2014.

[7] Y. Kieffel, A. Girodet, F. Biquez, P. Ponchon, J. Owen, M. Costello, M. Bulinski, R. Van San and K. Werner, “SF6 Alternative Development for High Voltage Switchgears,” *CIGRE Technical Brochure*, Vols. D1-305, 2014.

[8] L. Christophorou, J. Olthoff and D. S. Green, “Gases for Electrical Insulation and Arc Interruption: Possible Present and Future Alternatives to Pure SF6,” U.S Department of Commerce, Washington , 1997.

[9] L. Christophorou and R. Van Brunt, “SF6/N2 Mixtures: Basic and HV Insulation Properties,” *IEEE Transactions on Dielectrics and Electrical Insulation,* vol. 2, no. 5, pp. 952-1003, 1995.

[10] M. Zhou and J. Reynders, “Synergy between SF6 and Other Gases to Enhance Dielectric Strength,” in *10th International Symposium on High Voltage Engineering*, Montreal, 1997.

[11] W. Sun, Y. Li, D. Zheng, R. Guo and X. H. Du, “Insulation Characteristics of SF6/N2 Gas Mixtures and Applied Researches,” in *IEEE Annual Report Conference on Electrical Insulation and Dielectric Phenomena*, 2013.

[12] M. Rabie and C. Franck, “Predicting the Electric Strength of Proposed SF6 Replacement gases by Means of Density Functional Theory,” in *International Symposium on High Voltage Engineering 2013*, Zurich, 2013.

[13] L. Christophorou, I. Sauers, D. James, H. Rodrigo, M. Pace, J. Carter and S. Hunter, “Recent advances in Gaseous Dielectrics,” *IEEE,* Vols. EI-19, no. 06, pp. 550-566, 1984.

[14] L. Christophorou, D. James and R. A. Mathis, “On the Role of Electron Impact Ionisation and Electron Scattering Cross-Section in the breakdown Strength of Dielkectric Gases,” *J. Phys. D: Appl. Phys.,,* vol. 12, pp. 1223-1236, 1979.

[15] M. Zhou and J. Reynders, “AC and Negative Lightning Impulse Voltage Breakdown Characteristics of Gas Mixtures in a Coaxial Cylinder Gap,” in *7th Proceedings of the Southern African Universities Power Engineering Conference*, Johannesburg, 1998.

[16] Y. Qiu and Y. Feng, “Investigation of SF6-N2, SF6-CO2 and SF6-Air Substitutes for SF6 Insulation,” in *IEEE International Symposium on Electrical Insualtion*, Montreal, 1996.

[17] A. Swanson, “Investigation into the Role of Ions and Excited Molecules in the Corona Process in Air,” Univesity of the Witwatersrand, Johannesburg, 2015.

[18] P. Osmokrovic, M. Stojkanovic, K. Stankovic and M. Vujisic, “Synergistic Effect of SF6 and N2 Gas Mixtures on the Dynamics of Electrical Breakdown,” *IEEE Transactions on Dielectrics and Electrical Insulation,* vol. 19, no. 2, pp. 677-688, 2012.

[19] Z. Rajovic, M. Vujisis, K. Stankovic and P. Osmokrovic, “Influence of SF6-N2 Gas Mixture Parameters on the Effective Breakdown Temperature of the Free Electron Gas,” *IEEE Transactions on Plasma Science,* vol. 41, no. 12, pp. 3659-3665, 2013.

[20] M. Zhou, J. Reynders and S. Nielsen, “The Basic Physical Process in Gas Breakdown,” University of the Witwatersrand, Johannesburg.

[21] V. J. Kluss, “Measuring Picosecond Flashover in Pressurised Sulfur Hexaflouride (SF6),” Aalto University, Espoo, 2011.

[22] L. Christophorou and L. Pinnaduwage, “Basic Physics of Gaseous Dielectrics,” *IEEE Transactions on Electrical Insulation,* vol. 25, no. 1, pp. 55-74, 1990.

[23] L. Christophorou, “Electronegative Gases,” *Physics,* 1989.

[24] L. Christophorou and R. Van Brunt, “SF6/N2 Mixtures,” *IEEE Transactions on Dielectrics and Electrical Insulation,* vol. 2, no. 5, pp. 952-1003, 1995.

[25] E. Kuffel, W. Zaengal and J. Kuffel, High Voltage Engineering Fundamentals, Butterworth-Heinemann, 2000.

[26] D. Go, “Ionisation,” in *Gaseous Ionisation and Ion Transport: An Introduction to Gas Discharges*, University of Notre Dame, 2012, pp. 1-30.

[27] M. Naidu and V. Kamaraju, High Voltage Engineering Second Edition, McGraw-Hill, 1995.

[28] M. Macken, “Modelling and Simulations of Corona Discharge Currents in a Large Scale Coaxial Geometry with a Dielectric Barrier due to Low Frequency Triangular Voltages,” Chalmers University of Technology, Gothenburg, 2014.

[29] J. Holtzhausen and W. Vosloo, High Voltage Engineering Practice and Theory.

[30] C. S. Pradhan, “Simulation of Air Breakdown using Different Electrodes,” National Institute of Technology, Rourkela, 2011.

[31] A. Pederesen, “Calculation of Spark Breakdown or Corona Starting Voltages in Nonuniform Fields.,” *IEEE Transactions on Power Apparatus and Systems,* Vols. PAS-86, no. 2, pp. 200-206, 1967.

[32] A. Cookson, “Review of High-Voltage Gas Breakdown and Insulators in Compressed Gas,” *IEEE,* vol. 128, no. 4, pp. 303-312, 1981.

[33] A. Pedersen, “The Effect of Surface Roughness on Breakwon in SF6,” *IEEE Transactions on Power Apparatus and Systems,* Vols. PAS-94, no. 5, pp. 1749-1754, 1975.

[34] A. Mahdy, “Assesment of Breakdown Voltage of SF6/N2 Gas Mixtures under Non-uniform Field,” *IEEE Transactions on Dielectrics and Electrical Insulation,* vol. 18, no. 2, pp. 607-612, 2011.

[35] S. El-Makkawy, “Electrode Surface Roughness Initiated Breakdown in Compressed SF6 Gas,” *IEEE Annual Report ,* pp. 948-953, 1994.

[36] M. Farsadi and O. Kalenderli, “Effect of Macroscopic Electrode Surface Roughness on Breakdown and Corona Inception Voltages in SF6+N2 Gas Mixtures,” 2003.

[37] F. Endo and T. Kichikawa, “Dielectric Characterisitcs of SF6 Gas for Application to HVDC Systems,” *IEEETransactions on Pwer Apparatus and Systems,* Vols. PAS-99, no. 3, pp. 847-855, 1980.

[38] S. Haq, “Electron Collision Cross-Sections in Mono-Silane Molecule: An Investigation and Analysis,” IEEE, Ontario, 2005.

[39] Phelps Database, “LXcat,” [Online]. Available: http://www.lxcat.laplace.univ-tlse.fr. [Accessed 4 June 2013].

[40] A. Settaouti and L. Settaouti, “Simulation of Electron Swarm Parameters in SF6,” pp. 121-136, 2004.

[41] G. Hagelaar and L. Pitchford, “Solving the Boltzmann Equation to Obtain Electron Transport Coefficients and Rate Coefficients for Fluid Models,” *Plasma Sources Science and Technology,* vol. 14, no. 4, pp. 722-733, 2005.

[42] L. Wei, D. Yuan, Y. Zhang and Z. Tan, “Electron Drift, Diffusion and Effective Ionisation Coefficients in SF6-CHF3 and SF6-CF4 Mixtures from Boltzmann Analysis,” in *20th International Conference on Gas Discharge and Their Applications*, Orleans, 2014.

[43] Y. Qiu and D. Xiao, “Ionisation and Attachment Coefficients Measured in SF6/Ar and SF6/Kr Gas Mixtures,” *Journal of Physics D: Applied Physics,* vol. 27, pp. 2663-2665, 1994.

[44] J. De Urquijo, M. Yousfi, A. Juárez, A. Bekstein, E. Basurto, M. Benhennis, J. Henrández-Ávila, O. Eichwald and N. Merbahi, “Electron Swarm Coefficients in CO2-Air Mixtures,” in *International Conference on Phenomena in Ionised Gases*, Cancún, 2009.

[45] J. Hernández-Ávila, E. Basurto and J. d. Urquijo, “Electron Transport and Swarm Parameters in CO2 and its Mixtures with SF6,” *Journal of Physics D: Applied Physics,* vol. 35, no. 18, p. 2264, 2002.

[46] J. De Urquijo, “Derivation/Validation of Collision Cross Sections for Ions and Electrons in Gases from Measured Swarm Coefficients,” *Momentum,* vol. 1.

[47] W. Hendrick, “An Apparatus for Measurement of Electron Attachment and Electron Swarm Drift Velocities at High Temperatures,” MSc Thesis; University of Tennessee, Oak Ridge, 1968.

[48] T. Vivaldini, I. Lima, J. Gonçalves, S. Botelho, M. Ridenti, P. Fonte, A. Mangiarotti, P. Pascholati and C. Tobias, “Measurements of Electron Drift Velocity in Pure Isobutane,” in *International Nuclear Atlantic Conference*, Rio de Janeiro,, 2009.

[49] X. Liu, J. Wang, Y. Wang, Z. Zhang and D. Xiao, “Analysis of the Insulation Characteristics of c-C4F8/CO2 Gas Mixtures by the Monte Carlo Method,” *Journal of Physics D: Applied Physics,* vol. 41, pp. 1-5, 2008.

[50] S. Yoshinaga, N. Y and M. Hayashi, in *25th Inernational Conference on Physics Ionised Gases*, Nagoya, 2001.

[51] R. Sierra, H. Brooks, A. Sommerer, S. Foltyn and K. Nygaard, “Effective Swarm Parameters and Transport Coefficients in CO2 Laser Mixtures,” *Journal of Physics D: Applied Physics,* vol. 14, pp. 1791-1801, 1981.

[52] F. Harris and G. Jones, *Journal of Physics B: Atomic Molecular Physics,* vol. 4, p. 1536, 1971.

[53] T. Aschwanden, *Gaseous Dielectrics,* vol. 4, p. 24, 1984.

[54] V. Lisovskiy and Y. V.D, “Electron Drift Velocity Determination in CF4 and SF6 in a Strong Electric Field from Breakdown Curves of Low Pressure RF Dsicharge,” *Journal of Physics D: Applied Physics,* vol. 32, pp. 2645-2648, 1999.

[55] Y. Itikawa, “Cross Sections for Electron Collisions with Nitrogen Molecules,” *Journal of Physics and Chemistry,* vol. 35, no. 1, pp. 32-53, 2006.

[56] Y. Itikawa, “Cross Sections for Electron Collisions With Carbon Dioxide,” *Journal of Physics and Chemistry,* vol. 31, no. 3, pp. 749-767, 2002.

[57] Y. Zhang, R. Zeng, X. Wang, B. Zhang and J. He, "Study on Initial Stage of Gas Discharge by Numerical Method," in *Progress In Electromagnetics Research Symposium*, Hangzhou, 2008.

[58] J. Guo and C. Wu, "Two-Dimensional Nonequilibrium Fluid Models for Streamers," *IEEE Transactions on Plasma Science*, vol. 21, no. 6, pp. 684-695, 1993.

[59] d. P. Lymberopoulos and D. J. Economou, "Fluid Simulations of Glow Discharges: Effect of Metastable Atoms in Argon," *Journal of Applied Physics*, vol. 73, no. 8, pp. 3668-3679, 1993.

[60] A. S. Bhangaonkar and S. Kulkarni, "Approaches for Numerical Simulation of Partial Discharges," *IEEE*, p. 572575, 2008.

[61] G. Georghiou, A. Papadakis and A. C. Metaxas, "Numerical Modelling of Atmospheric Pressure Gas Discharges Leading to Plasma Production," *Journal of Applied Physics D*, 2005.

[62] E. Eylenceoglu and I. Rafatov, "Two-dimensional Hybrid Model for a Glow Discharge: Comparison with Fluid and Kinetic (particle) Models, Reliability and Accuracy," *Journal of Physics.*

[63] S. Dhali and P. Williams, "Two-Dimensional Studies of Streamers in Gases," *Journal of Applied Physics*, vol. 62, no. 12, pp. 4696-4707, 1987.

[64] J. P. Boris and D. Book, "Flux-Corrected Transport. I. SHASTA, A Fluid Transport Algorithm That Works," *Journal of Computational Physiscs*, vol. 11, pp. 38-69, 1973.

[65] R. Morrow, "Theory of Negative Corona in Oxygen," *The American Physical Society*, vol. 32, no. 3, pp. 1799-1809, 1985.

[66] G. Georghhiou, R. Morrow and A. Metaxas, "A Two-Dimensional, Finite-Element Flux-Corrected Transport," *Journal Physics D: Applied Physics,* vol. 33, pp. 2453-2466, 2000.

[67] G. Georghiou, L. Papageorgiou and A. Metaxas, "Three-Dimensional Numerical Modelling of Gas Discharges at Atmospheric Pressure Incorporating Photoionisation Phenomena," *Journal of Physics D: Applied Physics,* vol. 44, pp. 1-10, 2011.

[68] R. Morrow, "A Survey of the Electron and Ion Transport Properties of SF6," *IEEE Transactions on Plasma Science,* Vols. PS-14, no. 3, pp. 234-239, June 1986.

[69] A. Davies, "Discharge Simulation," *IEE Proceedings,* vol. 133, no. 4, pp. 217-240, 1986.

[70] "Standard Test Method for Dielectric Breakdown Voltage and Dielectric Strength of Insulating Gases at Commercial Power Frequencies," ASTM D2477-02, 2007.

[71] L. I. Xudong, Z. Wei, T. Youping, Z. Guifeng and C. W, "Breakdown Characteristics of Binary Gas Mixtures SF6-N2 and SF6-CO2 Under 0.1~0.25 MPa Atmosphere Pressures," Beijing, 2009.

[72] A. Bogaerts, K. De Bleecker, I. Kolev and M. Madani, "Modelling of Gas Discharge Plasmas: What Can We Learn from It?," *Surface and Coatings Technology,* pp. 62-67, 2005.

[73] S. Meijer, J. Smit and A. Girodet, "Comparison of the Breakdown Strength of N2, CO2 and SF6 using the Extended Up-and-Down Method," in *Properties and Applications of Dielectric Materials, 8th International Conference*, 2006.

[74] N. Malik and A. Qureshi, "Breakdown Mehanisms in Sulphur Hexafluoride," *IEEE Trnas. Electr. Insul,* Vols. EI-13, no. 3, pp. 135-145, 1978.

[75] D. Koch, "SF6 Properties, and Use in MV and HV Switchgear," Schneider Electric, 2003.

[76] UNIPEDE, “Guide to the Safe Use of SF6 in Gas Insulated Electrical Equipment,” UNIPEDE, Brussels, 1998.

Appendix A Ion Mobilities and Diffusion

The reduced positive mobilities (μ_+^0) and the reduced negative mobilities (μ_-^0) of SF_6 are obtained from Morrow [68] and given in

Table 3 and Table 4 respectively. The actual mobility is given by [68]:

$$\mu_+ = \mu_+^0 \cdot \frac{P_0}{P} \cdot \frac{T}{T_0} \tag{37}$$

Where:

$$P_0 = 101.325 \text{ (kPa)}$$

$$T_0 = 293 \text{ (K)}$$

Table 3: Reduced Positive SF_6 Ion Mobility

E/N $(\mathrm{V \cdot m^2})$	$< 1.2 \times 10^{-19}$	$1.2 \times 10^{-19} < E/N < 3.5 \times 10^{-19}$	$> 3.5 \times 10^{-19}$
μ_+^0 $(\mathrm{m^2 \cdot V^{-1} \cdot s^{-1}})$	6.0×10^{-5}	$1.216 \times 10^{-5} \times \log_e(E/N) + 5.89 \times 10^{-4}$	$-1.897 \times 10^{-5} \times \log_e(E/N) - 7.346 \times 10^{-4}$

Table 4: Reduced Negative SF_6 Ion Mobility

E/N $(\mathrm{V \cdot m^2})$	$E/N < 5.0\ 10^{-19}$
μ_-^0 $(\mathrm{m^2 \cdot V^{-1} \cdot s^{-1}})$	$1.69 \times 10^{32} \times (E/N)^2 + 5.3 \times 10^{-5}$

A single value is required for the positive ion mobility and a single value for the negative ion mobility of SF_6. This value is calculated using the maximum value from a 0 to 500 Td range as shown in Table 5.

Table 5 SF_6 Ion Mobility

E/N (Td)	0	250	500
E/N $(10^{-19}\mathrm{V.m^2})$	0	2.5	5
μ_+ $(\mathrm{cm^2 \cdot V^{-1} \cdot s^{-1}})$	0.64	0.73	0.70
μ_- $(\mathrm{cm^2 \cdot V^{-1} \cdot s^{-1}})$	0.53	0.69	1.0

The diffusion of the ions are calculated using equation (9) and displayed in Table 6.

Table 6: Ion Diffusion

Diffusion of Positive SF_6 ion $(\mathrm{cm^2.s^{-1}})$	D_{ps}	1.9×10^{-2}
Diffusion of Negative SF_6 ion $(\mathrm{cm^2.s^{-1}})$	D_{ns}	2.5×10^{-2}
Diffusion of Positive N_2 ion $(\mathrm{cm^2.s^{-1}})$	D_{pn}	3×10^{-2}
Diffusion of Negative N_2 ion $(\mathrm{cm^2.s^{-1}})$	D_{nn}	5×10^{-2}
Diffusion of Positive CO_2 ion $(\mathrm{cm^2.s^{-1}})$	D_{pc}	2×10^{-2}
Diffusion of Negative CO_2 ion $(\mathrm{cm^2.s^{-1}})$	D_{nc}	2.5×10^{-2}

Appendix B Selection of the Experimental Parameters

There were three factors considered in choosing the experimental pressures of the gas mixture. Firstly, could the apparatus handle the pressure? While the pressure chamber was designed for test pressures up to 650 kPa the chamber is old so it was decided best to add a safety factor of 2 to the original maximum test pressure. This resulted in a maximum test pressure of 325 kPa which was rounded down to 300 kPa for uniformity in pressure increases. The second consideration was whether the impulse generator could supply a sufficiently high voltage to cause breakdown in pure SF_6 at the maximum pressure for the standard gap distance. The third and final consideration was whether these pressures were within the working pressure range for electrical equipment. According to UNIPEDE SF_6 gas in electrical equipment is normally at absolute pressures of 100 kPa to 900 kPa [76] so a pressure range from 100 kPa to 300 kPa is sufficient to determine whether a SF_6 mixture would be a suitable replacement for pure SF_6.